Nanoscale Horizons

REVIEW

View Article Online
View Journal

Cite this: DOI: 10.1039/d5nh00009b

A microscopic view of solid-state lithium batteries

Mohamad Khoshkalam, *[a] Fardin Ghaffari-Tabrizi [a] and Dennis Valbjørn Christensen *[ab]

The demand for safe energy storage with high energy density is growing, and as conventional lithium-ion batteries with liquid electrolytes are nearing their performance limits, solid-state Li batteries have emerged as promising successors. Solid-state batteries offer higher energy density, enhanced safety, and faster charge rates. However, their commercialization remains constrained by solid/solid interface processes, including dendrite formation, chemically or mechanically unstable electrolyte/electrode interfaces, and inhomogeneous cathodic reactions. Advanced micro- and nanoscale characterization techniques are essential for unveiling the mechanistic origins of solid-state battery degradation and performing real-time monitoring of local changes within battery materials, which reveal critical insights into dynamic interfacial processes during operation. Such knowledge may unlock the full potential of solid-state batteries by guiding the development of new materials, battery architectures, and microstructures for achieving improved performance and durability. This review surveys research on solid-state battery materials and examines how various micro- and nanoscale characterization techniques can be used to diagnose degradation phenomena and develop strategies to mitigate degradation. We review recent studies with a particular focus on (i) grain and phase boundaries in solid-state electrolytes, (ii) dendrite formation, (iii) the structure and evolution of solid electrolyte interphases, (iv) lithiation-induced heterogeneities in the anode active materials, (v) cathode electrolyte interfacial phenomena, and (vi) contact loss within cathode composites and the resulting spatial heterogeneities revealed through state-of-charge mapping. Finally, we discuss how future developments in characterization methods can enable gaining a deeper insight into the operation and degradation of solid-state batteries.

Received 6th January 2025,
Accepted 24th September 2025

DOI: 10.1039/d5nh00009b

rsc.li/nanoscale-horizons

[a] *Department of Energy Conversion and Storage, Technical University of Denmark, Anker Engelunds Vej, DK-2800, Kgs. Lyngby, Denmark. E-mail: mokhos@dtu.dk, dechr@dtu.dk*

[b] *Institute for Advanced Study (IAS), Technical University of Munich, Lichtenbergstraße 2 a, 85748, Garching, Germany*

Mohamad Khoshkalam

I am a Development Engineer at the Technical University of Denmark, working in the field of battery materials. Trained as a materials scientist, I apply fundamental electrochemistry together with advanced materials synthesis and characterization to the development of electrochemical devices for applications in energy storage and conversion. My current research focuses on degradation mechanisms and structure–property relationships in layered oxides for Li- and K-ion batteries.

Fardin Ghaffari-Tabrizi

I am a second-year PhD student at the Technical University of Denmark (DTU). I studied Aerospace Engineering at RWTH Aachen before moving into the field of energy storage. My research focuses on advancing solid-state batteries by employing magnetic imaging with Nitrogen-Vacancy (NV) centers in diamonds. Using Scandinavia's first NV magnetometer, I investigate critical failure mechanisms such as dendrite formation and inhomogeneous current flow at the nanoscale. By providing new insights into how these batteries operate and fail, my work aims to accelerate the development of safer and lighter energy storage technologies.

1. Introduction

Conventional lithium-ion batteries (LIBs) with liquid electrolytes are widely regarded as the most robust electrochemical energy storage technology, serving a variety of sectors including electrification of transportation and grid-scale applications.[1,2] LIBs are valued for their reliable performance, long lifespan, and high cycling capability, as well as their notable energy and power densities.[1,2] Since Sony's first demonstration in 1991, the commercial success and scalability of LIBs have resulted in a doubling of specific energy and energy density, now reaching up to 270 Wh kg^{-1} and 650 Wh L^{-1}, respectively.[2] Concurrently, the production cost of LIBs has plummeted by an impressive 98% to lower than 100 USD per kWh.[2] However, current projections suggest that LIBs are approaching their peak performance while the demand for energy storage solutions with higher safety and energy density grows.[2] This motivates exploring alternative technologies as potential successors to LIBs.[3] In this context, the development of solid-state Li batteries (SSBs), in which the flammable liquid electrolyte is replaced with a solid-state electrolyte (SSE), is proposed as one of the most significant steps in transitioning from LIBs to the next generation of batteries.[1,3] The SSB technology has the potential to offer various advantages over conventional LIBs, including higher energy and power density, safe operation without flammable liquid electrolytes, prevention of cross-talk between electrodes, a wider operating temperature range, and faster charging rates.[1] However, to date, there has been limited evidence demonstrating the full potential of SSB technology for commercial applications.[1–3] Several reasons, such as high stacking pressure required for stable long-term operation[1] and the difficulty as well as the high cost of scaling up manufacturing of SSEs,[4] are among the major contributors. However, the root cause of many scientific and technical challenges hindering the full utilization of SSB technology can be summarized in one word: interfaces. Fast charge transport across the interfaces between the SSEs and electrodes, combined with stable chemical and mechanical interactions, is vital for achieving long-term, reliable performance in SSBs. Yet, many of these interfaces suffer from issues that significantly restrict the performance of the batteries.

To unlock the full potential of SSBs, it is essential to thoroughly understand the mechanisms driving interfacial degradation and use this knowledge to develop improved material chemistries, structures, and architectures. However, the buried nature of many of these phenomena, coupled with their microscopic origin, hinders the effective utilization of conventional material characterization and electrochemical techniques, which are often only sensitive to the macroscale or surface-near regions. Local characterization is thus crucial for devising strategies that mitigate degradation, enhance efficiency, and ensure durability in SSBs.[3] Here, we present recent progress in micro- and nanoscale characterization techniques applied on SSBs to gain insights into solid-state processes as well as degradational phenomena in battery materials. Initially, a succinct overview of SSBs will be provided, highlighting the solid-state processes occurring within their components, materials, and interfaces. Following this, various microscopic characterization techniques will be briefly introduced. Building on these foundational elements, we highlight recent progress in applying micro- and nanoscale characterization techniques to unravel key processes governing the performance and stability of SSBs. These include: (i) the role of grain and phase boundaries in SSEs, (ii) the formation and propagation of dendrites, (iii) the structure and evolution of solid electrolyte interphases (SEIs), (iv) lithiation induced heterogeneities in anode active materials, (v) interfacial phenomena at cathode electrolyte interfaces (CEI), and (vi) contact loss within the cathode composite layer, and the development of chemical and electrochemical heterogeneities in cathode layers as revealed through state-of-charge mapping.

Dennis Valbjørn Christensen

Congratulations on the 10th anniversary and best wishes for the decade to come. As a nanoscientist working on understanding, tailoring, and visualizing processes at the nanoscale at the Technical University of Denmark, Nanoscale Horizons stands out as one of the top journals for my research. My research resonates particularly well with the strong focus on innovative nanoscience and technology. I have been pleased to both act as a community board member for Nanoscale Horizons for the past two years and contribute an article to the 10th anniversary special collection.

2. Solid state batteries

In SSBs, the liquid electrolyte is replaced by a SSE, which offers several potential key advantages over conventional LIBs, positioning these solid-state electrochemical devices as a potential "holy grail" of next-generation energy storage solutions.[1] However, this replacement also transforms liquid/solid interfaces into solid/solid ones, which introduces numerous challenges.[1,2] Most importantly, the robust contact and fast transport kinetics of ionic charge carriers in liquid electrolyte-based systems are generally replaced by slow transport kinetics in mechanically and electrochemically poorly contacted solid/solid interfaces, leading to undesirable effects on battery performance and lifespan.[1,2] Even though fast ionically conducting SSEs are being developed, the benefits are still not high enough to overcome the kinetically sluggish nature of the solid/solid interfaces.[2,4] These buried solid/solid interfaces are challenging to probe due to their limited accessibility using conventional characterization tools. Nonetheless, they serve as critical

hotspots where dynamic processes drive degradation in battery performance.[5] Therefore, the identification and characterization of these processes are key to realizing a long lifetime in SSBs.

Solid/solid interfaces and their associated degradation processes can be categorized into three main groups: (i) solid-state processes within SSEs, (ii) anode/SSE interfaces, and (iii) cathode/SSE interfaces, each presenting distinct properties and challenges. We will explore these interfaces and their issues in detail in the following sections.

2.1. Solid-state processes within SSEs

Solid-state processes at the internal interfaces in SSEs play a significant role in determining the ionic conductivity, mechanical stability, and material cost.[1,6] Fig. 1 illustrates some of these key interfacial features, including distinct grain boundary properties relative to the bulk material as well as phase boundaries between different phases in hybrid organic–inorganic electrolytes. In inorganic SSEs, grain boundaries are typically the primary paths for electronic leakage due to their high electronic conductivity and reduced band gap, making these interfaces preferential sites for metal plating.[7] At the same time, ionic transport across grain boundaries often limits the overall ionic conductivity of the SSEs.[8] A deeper understanding of the dynamics behind ionic and electronic transport along and across grain boundaries can offer valuable insights for enhancing the ionic conductivity, preventing plating of inactive metal islands within SSEs, and ultimately help avoid short-circuiting caused by dendrites.[6,7,9] Dendrites and filaments are often used interchangeably,[10] but in this manuscript we adopt the use of dendrites, as they are the more common terminology despite their physical geometries may include non-dendritic morphologies such as mosses, whiskers, and globules.[11] In addition to grain boundaries, phase boundaries are particularly important in hybrid organic–inorganic composite electrolytes, where the confined contact area between the polymers and inorganic compounds acts as the primary pathway for ion conduction.[6,9] Furthermore, similar to the grain boundaries in inorganic compounds, these phase boundaries also facilitate non-uniformities in electronic current leakage, which can lead to dendrite formation *via* the same mechanism.[6,9]

2.2. Anode/SSE interface

The potential use of high-capacity anodes with low potentials, such as Li–metal or silicon-based alloys, is considered one of the major advantages of SSB technology compared to LIBs.[1] These anodes enable higher energy density and faster charge/discharge rates.[1] However, the use of Li–metal or alloys comes with significant drawbacks that can limit the reversible operation and lifespan of SSBs, especially at high current densities.[1] Fig. 1 illustrates some of these interfacial degradation phenomena, including volume changes in the anode active material and the associated microcracking, and inhomogeneous metal plating leading to dendrite and pore formation, as well as the formation of an insulating SEI. One of the most critical issues in both Li–metal and silicon-based anodes is the high volume changes at the anode/SSE interface during charge/discharge cycles, which can lead to mechanical degradation and microcracking due to the solid/solid nature of the interface.[1,12,13] Additionally, inhomogeneous metal plating and stripping cause uneven current distribution, pore formation, and nucleation sites for dendrites, which can eventually short-circuit the battery.[12] While dendrite growth is generally considered less prevalent in SSEs than in conventional batteries with liquid electrolytes, it remains a major degradation mechanism in SSBs.[12] Some studies even argue that, due to the widespread use of Li–metal anodes in SSBs, dendrite growth may pose greater challenges in these cells compared to conventional LIBs.[14–16] The adverse effects of both dendrite growth as well as volume changes can be mitigated by applying high stack pressure to maintain mechanical integrity of the anode/SSE interface and reduce uneven current distribution, but this approach increases the cost and complexity.[1,2] Another approach is to use Li–alloys, interfacial layers, or anode scaffolds that can accommodate volume changes while simultaneously distributing the current more evenly.[1,17] Furthermore, many SSE materials, such as halides, thiophosphates, and even oxides, are chemically incompatible with Li–metal, leading to the formation of SEIs.[1,18,19] The SEIs are often insulating and consequently increase cell resistance and reduce battery performance.[1,18,19] However, SEI formation is a complex phenomenon that can produce interfacial phases with a wide range of ionic and electronic conductivities. Some SEIs, such as those formed by the reduction of cations like Ge^{4+} and Ti^{4+} to their metallic form, are highly electronically conductive and thus continue to grow unchecked during operation.[20]

2.3. Cathode/SSE interface

Due to the relatively poor ionic and electronic conductivity in cathode active materials (CAMs) and inadequate interfacial properties, the cathode layer is typically a composite material.[21] This composite includes CAMs, an electronic conductor such as carbon-black, an ionic conductor like SSE, and other potential additives or binders. As shown schematically in Fig. 1, both the highly ionic conducting SSE and high-capacity anode layers are relatively thin compared to the composite cathode layer.[1] As a result, the cathode layer dominates the SSB cell in terms of volume, weight, and the number of interfaces.[1] Simultaneously, due to the use of high-capacity Li–metal anodes, the cell capacity is usually bottlenecked by the lower theoretical capacity of CAMs. This is because the total amount of charge a battery can store depends on the electrode that holds the least charge. While Li–metal can store a very large amount of Li^+, the cathode can only accommodate a smaller number of ions, effectively limiting the overall capacity of the cell. These factors eventually determine the specific energy and energy density of the cell, as both scale with the overall cell's capacity, and are inversely related to the cell's weight and volume, respectively.[1] Similar to conventional batteries using liquid electrolytes, the functionality of CAMs in terms of reversible lithiation/delithiation is of utmost importance for the stable cycling of SSBs.[21,22] During cycling, most of the

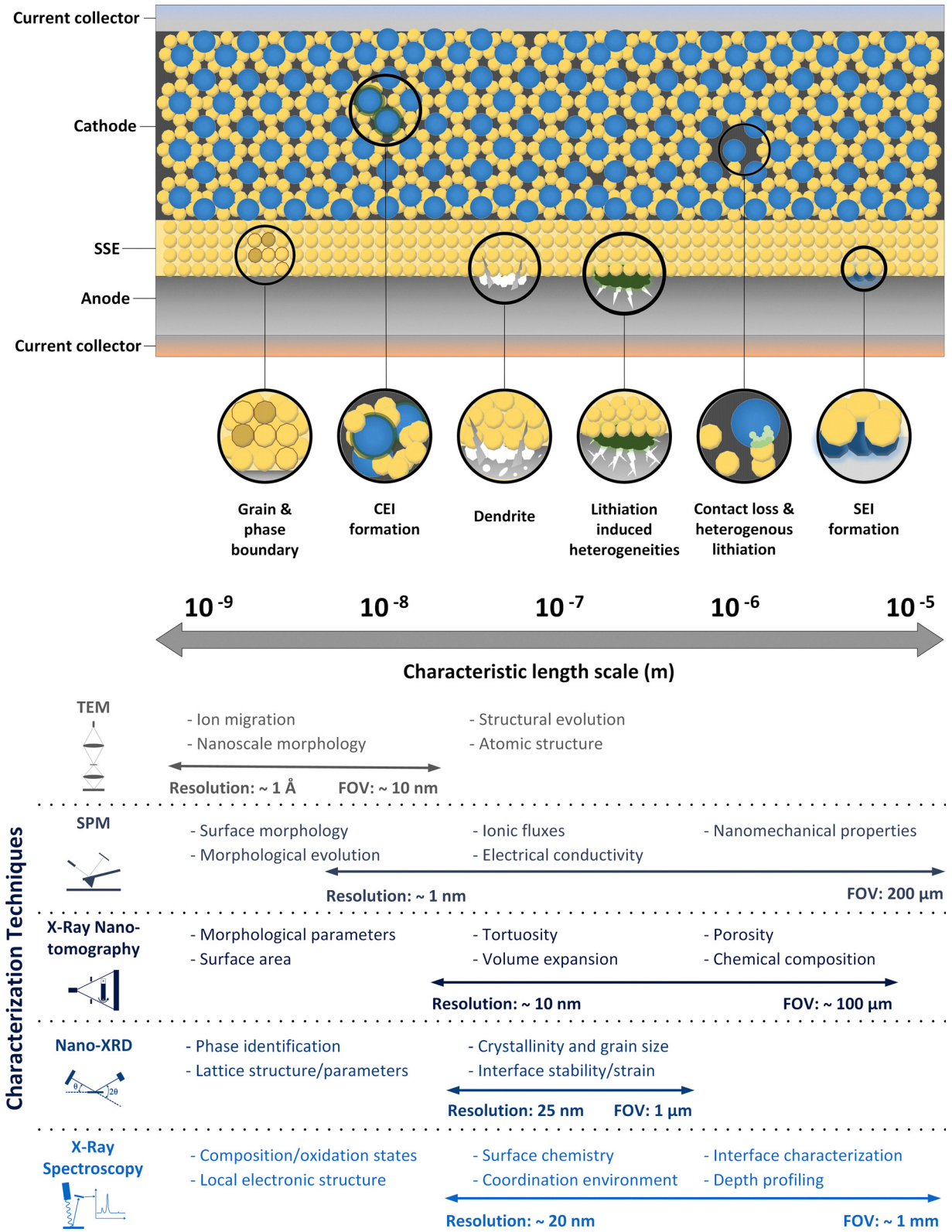

Fig. 1 Overview of interfacial degradation phenomena in solid-state batteries along with their approximate characteristic length scales and the most relevant micro- and nanoscale characterization techniques. Each technique is detailed with its specific applications and properties it can assess in solid-state battery research, along with information about its resolution and typical high-resolution field of view. References for the individual techniques are provided in Table S1 in the SI.

existing CAMs go through a considerable amount of volume change, although comparatively smaller than anode active materials.[1] In batteries with liquid electrolytes volume changes can be mitigated by the ability of the CAM to easily move through the liquid.[23] However, due to the solid/solid nature of the CAM/SSE interface, the same volume change can cause a significant amount of local strain, which deteriorates the mechanical integrity of the cathode layer by crack formation and contact loss, as shown in Fig. 1.[1,23] Additionally, the formation of a CEI also plays a critical role in determining the SSB performance as it introduces changes in interfacial ionic and electronic transport. Interdiffusion of ionic species, *e.g.* transition metals between the SSE and CAM particles, occurring primarily during fabrication or sintering, further affects the overall battery efficiency.[21,24] Therefore, the chemical compatibility of SSEs and CAMs is among the most important parameters to consider during the material selection stage.[21] To achieve high-performance SSBs, it is crucial to develop a comprehensive understanding of the chemical and physical properties at the cathode/electrolyte interface. Equally important is the ability to maintain fast ion and electron transport across this interface, which is often more critical than simply combining the fastest SSE with a high-capacity CAM.[23]

3. Micro- and nanoscale characterization techniques

Several categories of micro- and nanoscale characterization techniques have been used for investigating battery materials, interfaces, components, and processes. The main groups include electron-based,[3,25] light-based,[25–27] and scanning probe-based[5,28–30] techniques. Techniques based on magnetic fields, such as nuclear magnetic imaging, are also gaining popularity, but they often lack the resolution to spatially resolve the local processes[31] with a few exceptions such as scanning magnetometry.[32] Most microscopy techniques represent a trade-off between a large field-of-view and a high spatial and temporal resolution, and often require specialized sample preparation or synchrotron access.[25] The methods can be used post-mortem, *in situ*, or *operando*, revealing temporal information regarding the evolution of material structures, interfaces, and kinetic processes during battery operation.[5] The ideal *in situ* or *operando* measurement setups should be capable of penetrating standard pouch or stainless steel encased cells without requiring sophisticated modifications while also being non-invasive and offering high spatial and temporal resolution.[25]

In SSB research, utilization of advanced micro- and nanoscale characterization techniques and upgrading existing techniques with enhanced functionality are essential to understand and optimize battery performance.[3] Among the prominent methods, light-based techniques, such as X-ray computed tomography (CT), scanning transmission X-ray microscopy (STXM), and X-ray absorption near edge structure (XANES) spectroscopy, offer unique advantages.[5] These techniques enable high-resolution 3D morphological reconstruction down to 10 nm spatial resolution,[27] allowing researchers to probe the chemical evolution of the compounds, tracking Li^+ migration, assess valence state variations, heterogeneities inside and between electrode active materials,[33–35] as well as *in situ* monitoring of active material volume changes.[5,6,26,27] Despite their power, these techniques often rely on synchrotron sources, which present technical challenges and limited accessibility for broader research use in addition to the potentially invasive nature of the intense light source and the weak scattering properties of light elements such as Li.[5,6,26,27,36–38]

Electron-based techniques also play a critical role in capturing fine structural and compositional details down to sub-atomic spatial resolution.[3,26] These techniques have been employed to investigate mechanical interactions at interfaces,[39] observe chemical and structural changes,[40–43] and study dendrite formation *in operando*.[39,43,44] However, limitations arise due to the sensitivity of Li to electron beams, its low scattering cross-section, the shallow penetration depth of electrons in solid materials, and the need for complex and invasive sample preparation for transmission experiments.[45] Cryogenic transmission electron microscopy (Cryo-TEM) is particularly valuable for observing electrochemical processes without extensive sample damage, though beam sensitivity remains a challenge.[46] Focused ion beam coupled with scanning electron microscopy (FIB–SEM), especially with recent advancements in Xe^+ plasma FIB for large-volume sectioning, supports detailed tomographic analysis and is indispensable for investigating SSB local structures with spatial resolutions below 1 nm.[47]

Scanning probe techniques provide additional insights into surface properties, which aid in the characterization of micro- and nanoscale properties such as local mechanical and electrochemical properties.[5] With a horizontal resolution of 1–10 nm[5,29] and a vertical resolution of a few angstroms (Å),[29,48] atomic force microscopy (AFM) can precisely map surface morphology and track its changes during cycling. AFM has also been proven useful in studying adhesion and Young's modulus in hybrid electrolytes[6] and evaluating local electrochemical strain.[5] Additionally, scanning probe techniques with an electronically conducting probe can offer information on local ionic/electronic conductivity and space charge layers.[49] Key limitations of AFM include its inability to provide chemical information and being limited to surface imaging.[29,48] Furthermore, some processes occur on time scales too short for conventional low-speed AFM to image.[48] Therefore, advancing to high-speed AFM imaging while retaining high spatial resolution and employing multi-modal techniques such as AFM coupled with Raman (AFM-Raman) or infrared spectroscopy (AFM-IR) would offer significant advantages.[5,48] Multi-modal detection of current distributions and redox reactivity with subsurface sensitivity was also proposed using a scanning probe equipped with an atomic-sized magnetic field sensor.[32]

Currently, no single technique fulfills all the essential requirements for micro- and nanoscale SSB analysis. These include visualizing both electron and ion transport,

differentiating chemical states like metallic Li from Li^+, capturing processes across length scales from nanometers to 50 μm, resolving real-time dynamics, non-invasively extracting subsurface information, and identifying spatial features critical to SSB performance. Consequently, a comprehensive approach involving a combination of experimental techniques, theoretical modeling, and post-mortem analysis is necessary to reveal the complex inner workings of SSBs. Furthermore, the integration of multimodal methods, such as AFM-Raman, AFM-IR and scanning magnetometry, into battery research represents an exciting frontier.[5,32] By pairing many of these multimodal approaches with artificial intelligence (AI)-driven analysis, researchers can develop comprehensive models to better understand electrode microstructures, material heterogeneity, and their impacts on cell performance. This will ultimately support the design of more efficient battery architectures.[27] A summary of selected battery microscopy techniques for SSB research is presented in Fig. 1, which also displays their spatial resolution and field-of-view. For further details and in-depth information, readers are encouraged to consult the following review papers.[3,5,25,27,47,50–52]

4. A microscopic view of SSBs

The characterization of micro- and nanoscale processes in SSBs has significantly impacted the battery field by providing insight into the mechanistic origins underpinning both functional and degraded SSBs. This section reviews recent progress in various micro- and nanoscale studies investigating the interfacial processes in SSBs depicted in Fig. 1 by sequentially focusing on the SSEs, anodes, and cathodes.

4.1. SSEs

The two main types of interfaces present in SSEs are grain boundaries in inorganic materials and phase boundaries in hybrid organic/inorganic composites. Although Fig. 1 illustrates powder-pack based inorganic SSEs that are widely studied in the literature, this review also considers polymer electrolytes and hybrid organic/inorganic composites due to their emerging relevance and potential for enabling scalable SSB designs.

4.1.1. Grain boundaries. Grain boundaries within SSEs are considered to be bottlenecks for ionic transport kinetics and the key sites for degradational processes like dendrite growth.[6] One of the significant challenges in high-performance SSEs such as lithium lanthanum zirconium oxide (LLZO) is to understand the mechanistic origin of preferential propagation of dendrites through grain boundaries, which requires a thorough multi-scale insight.[7] Due to the nanometer size nature and short time scale of most of these processes, high spatial resolution and *in situ*/*operando* methods are required.[7] Liu *et al.*[7] combined *in situ* transmission electron microscopy (TEM) with techniques such as electron energy loss spectroscopy (EELS) to explore the mechanisms involved in this process.[7] The study was conducted on a hot-pressed disc of LLZO, which was galvanostatically cycled beyond the critical current density to short-circuit two Li–metal electrodes.[7] Although no secondary or amorphous phases were detected in the grain boundaries of LLZO, these interfaces were found to differ significantly from bulk grains in terms of their crystal structure, exhibiting high-index surfaces with complex orientations and higher atomic irregularities.[7] Such complex crystallographic orientations often result in increased reactivity and distinct electronic or ionic properties.[7] Additionally, local band gap measurement using EELS (Fig. 2A) revealed that the grain boundaries exhibited lower band gap values of 1–3 eV compared to 6 eV observed in LLZO grains.[7] This phenomenon resulted in increased electron conduction and preferential leakage of electronic current through the grain boundaries. The excess electron availability, along with the reduced grain boundary potential, facilitates island-like Li–metal plating along the grain boundaries, ultimately causing a short-circuit through dendrite growth during battery cycling.[7] This mechanistic origin complements other proposed mechanisms for dendrite-induced short-circuits in SSBs, such as heterogeneous Li–metal plating/stripping and mechanical crack propagation at the SSE/anode interface.[7,44] To date, there is still no consensus on how dendrites form in SSBs, which highlights a need for further *operando* nanoscale characterization.

Grain boundaries in SSEs have also been studied by electrochemical strain microscopy.[28] Electrochemical strain microscopy involves bringing a conductive tip on a cantilever in contact with the surface of the sample, applying an alternating voltage and using the resulting cantilever vibration to measure the strain response.[28] This localized strain response is attributed to the accumulation or depletion of charge-carrying Li^+ underneath the tip due to the voltage perturbation.[28] The resulting vibration amplitude has a linear correlation with both the local concentration of charge carriers as well as their diffusivity.[53] Since the relaxation time constant depends solely on the diffusivity of charge carriers, it allows for the decoupling of local ionic conductivity from charge concentration.[53] This phenomenon makes electrochemical strain microscopy particularly sensitive to variations in local ionic conductivity, allowing it to be used for mapping this parameter on the surface and examining its influence on degradational processes in SSBs.[28] Wang *et al.*[28] used electrochemical strain microscopy in order to assess the variations in the electrochemical response between the grain and grain boundaries in NASICON-structured $Li_{1.5}Al_{0.5}Ge_{1.5}(PO_4)_3$. Fig. 7B(a–c) shows that the electrochemical strain is markedly higher at the grain boundaries compared to the bulk grain. This observation was associated with the local accumulation of Li^+ at the grain boundaries and a slower transport kinetics at these intrinsic interfaces.[28] Such behavior highlights the importance of improving the grain boundary conductivity in $Li_{1.5}Al_{0.5}Ge_{1.5}(PO_4)_3$-based materials, a challenge that requires a different strategy to suppressing the electronic conductivity in LLZO grain boundaries.[28]

4.1.2. Phase boundaries. The emergence of hybrid SSEs has demonstrated that solid/solid polymer/ceramic interfaces

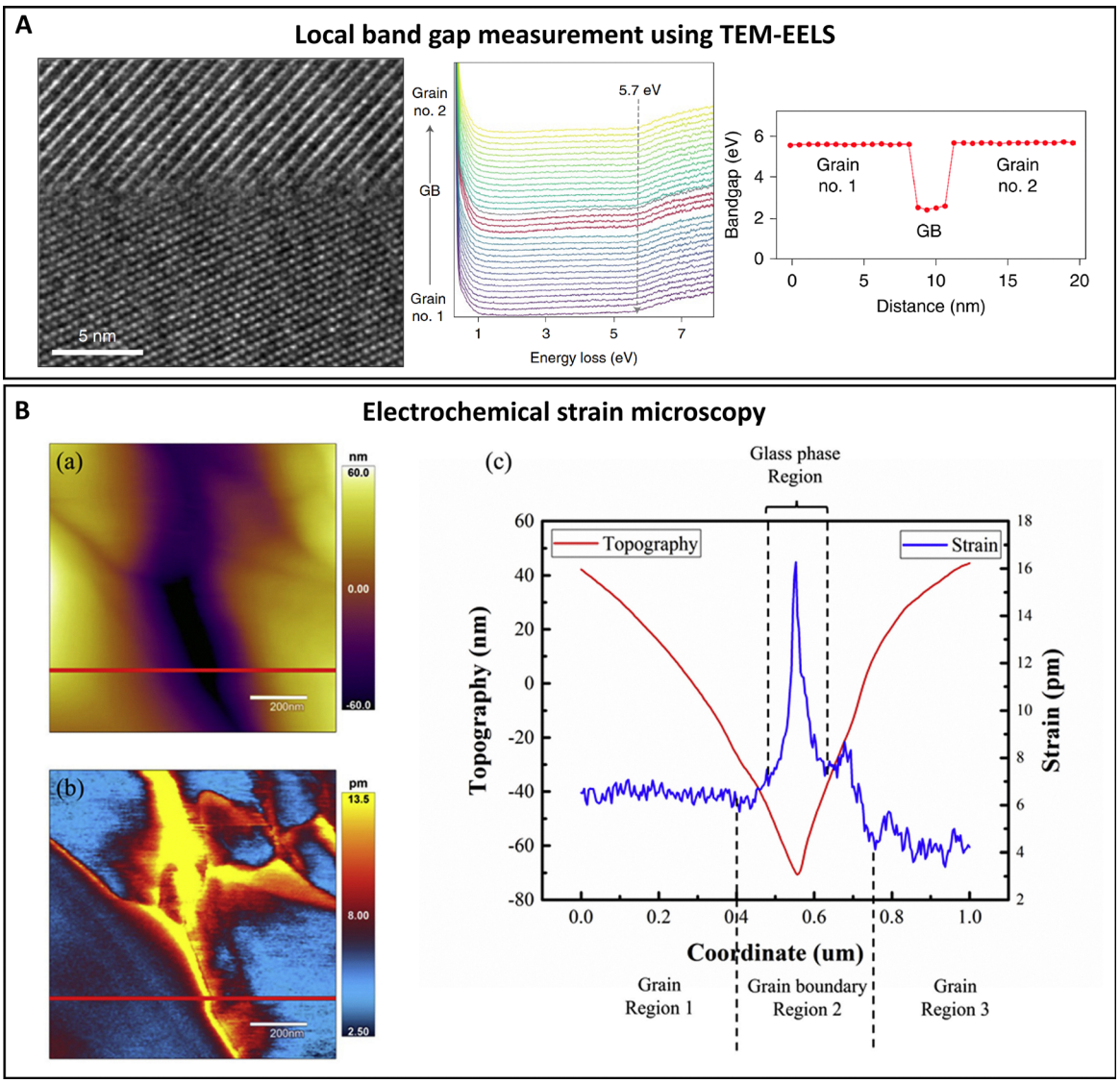

Fig. 2 Nanoscale characterization of grain boundaries in solid-state electrolytes. (A) High-resolution TEM image of an LLZO grain boundary, with a bandgap measurement of both the grain boundary and the adjacent grains. Adapted with permission from ref. 7, Copyright 2021 Springer Nature. (B) Characterization of $Li_{1.5}Al_{0.5}Ge_{1.5}(PO_4)_3$ using electrochemical strain microscopy as demonstrated in (a) topographic image, (b) distribution of electrochemical strain and (c) line analysis of topography and electrochemical strain performed on the red line illustrated in (a) and (b). Adapted with permission from ref. 28, Copyright 2020 Elsevier.

are critical spots for the initiation of chemical and mechanical instabilities during SSB operation.[6,54,55] Such instabilities are mostly determined by the nature of ionic transport within these interfaces, highlighting the necessity of micro- and nanoscale characterization to understand the kinetics involved.[6] The Lewis acid interactions between Li^+ and the functional groups in the polymer at the confined polymer/ceramic interface create conditions where transport kinetics differ significantly from those in the bulk polymer or inorganic SSE grains.[6] This phenomenon usually results in ionic pathways being controlled by these interfaces, which amplify the heterogeneity in ionic transport and redox reaction processes.[6] Such heterogeneity in ionic transport can be observed specifically at areas in which the hybrid electrolyte contacts the anode, and ultimately degrades the battery through various mechanisms including dendrite formation or augmented cell area-specific resistance.[6] Techniques with micro- and nanoscale spatial resolution, such as AFM and synchrotron X-ray nanotomography, are particularly valuable for providing mechanistic insights into these processes.[6,56] For instance, Dixit *et al.*[6] utilized AFM to map properties such as roughness, adhesion strength, and Young's modulus at interfaces between LLZO and polyethylene-oxide (PEO) of various molecular weights. PEO was mixed with LLZO and processed into an ink *via* ball milling and subsequently tape-cast into a 60 micrometer thick film.[6] The study concluded that smoother PEO/LLZO interfaces with low roughness in the range of 0.5–1 nm can enhance interfacial ionic transport kinetics by promoting a uniform concentration gradient

between the organic and inorganic sides of the interface.[6] In a similar study,[9] the ionic and electronic transport properties of Li_3PS_4 and its interface with polyimine were explored using a conductive AFM imaging setup (c-AFM). The study identified notable spatial variations in the ionic current of 1 to 2 orders of magnitude within Li_3PS_4.[9] These discrepancies arise from the differences in transport kinetics, which are strongly influenced by crystalline orientations in the polycrystalline and glassy Li_3PS_4.[9] Furthermore, the research highlighted that the ion transport behavior underwent a sharp shift at the boundary between the polymer and Li_3PS_4, which facilitates heterogeneous Li-metal plating/stripping. This heterogeneity is, in turn increasing the likelihood of dendrite formation at the Li-metal/hybrid–electrolyte interface.[9] An important implication is that, in addition to minimizing electronic conductivity at the grain boundaries or polymer/ceramic interfaces, tailoring microstructural properties to promote more uniform ion transport is also crucial for mitigating the growth of dendrites.[9]

4.2. Anodes

Fig. 1 provides a visual overview of the degradation mechanisms of the anode/SSE interface addressed in this section. These include dendrite formation, the development of a SEI, and degradation caused by lithiation induced volume expansion.

4.2.1. Dendrites. Tomography has proven to be an effective tool for visualizing phenomena such as dendrite growth, crack generation, temporal evolution of the Li/SSE interface morphology, and SEI formation.[57] The inclusion of stacking pressure as a variable in SSB characterization is crucial as sufficient pressure helps to mitigate dendrite formation and ensures that the Li-metal effectively wets the SSE in the gaps created during stripping.[58] When gaps form at the anode/SSE interface, uniform electrochemical plating in those regions during the next cycle becomes highly unlikely. As a result, Li-metal tends to accumulate at a few contact points, leading to localized spikes in current density and stress concentrations. These conditions promote dendrite nucleation and can ultimately result in its penetration into the SSE. Stacking pressure, along with the yield strength of Li-metal, the elastic modulus of the SSE, and the SSE porosity are key parameters in studies concerning dendritic short-circuiting.[58] Doux *et al.*[58] studied how the mechanical properties of the Li/Li_6PS_5Cl interface at varying stacking pressures influenced the cycle lifetime, as well as dendrite and SEI formation. After cycling the SSB cell at 25 MPa, the authors detected the propagation of low-density Li-metal dendrites through the grain boundaries of the SSE using tomography.[58] Simultaneously, diffraction patterns from the interface revealed the formation of a SEI containing LiCl and Li_2S phases, which was most likely located at the contact points between Li-metal and Li_6PS_5Cl.[58] This indicated that the SEI formation can occur alongside dendrite growth with both phenomena influencing the progression and suppression of each other.[58,59] Due to their high surface-to-bulk ratio, nanoscale dendrites promote interfacial reactions and convert a significant portion of Li-metal and SSE into inactive SEI phases, which leads to capacity loss and reduced coulombic efficiency.[60] The Li/Li_6PS_5Cl system was also investigated in another study using X-ray tomography and spatially resolved X-ray diffraction (XRD), focusing on the mechanical integrity of this interface and its effect on dendrite growth.[57] In this study, a symmetric Li/Li_6PS_5Cl/Li cell was cycled under constant current density and at fixed time intervals until short-circuiting occurred as a result of dendrite growth. The monochromatic X-ray beam was then aligned perpendicularly to the Li/Li_6PS_5Cl interface and scanned across the cell as shown in Fig. 3A. The {110} peak of Li-metal was then used to image the dendrite location with 3 μm spatial resolution.[57] The study also showed the complex interplay between the electrical field distribution, localized Li-metal plating, and conical crack formation at the interface.[57]

A combination of AFM and environmental-TEM has also been used for direct imaging of the dendrite nucleation and growth as displayed in Fig. 3B.[60] In this setup, an electrochemical cell was established using Li-metal as a counter electrode, exposing the Li-metal to air to form a LiO_2 surface layer serving as the SSE, and finally using a Ni-coated AFM tip as a working electrode. Electrochemical Li-metal plating on the AFM tip was performed under potentiostatic conditions. As the tip was in contact with the LiO_2 SSE, the growth of Li-metal on the tip and the resulting expansion of its volume exerted a force that pushed the cantilever away from the surface of the sample. This setup enabled simultaneous imaging of dendrite nucleation and growth (Fig. 3B(a–f)), electrochemical characterization during plating/stripping, and measurement of the resisting force against dendrite propagation.[60] The latter is measured *via* the bending force on the cantilever, which probes the mechanical resistance that an SSE exerts against dendrite growth.[60] The TEM-based electron diffraction analysis found that the dendrites grew through several consecutive growth modes. The first growth mode is a non-directional one, in which the nucleation process is controlled by the slow transport kinetics of Li^+ through the SSE and the minimization of surface energy, with a preference for {110} terminations (Fig. 3B, panels a–c). As the dendrite growth progresses, metal deposition transitions into a directional mode, terminating on the {112} plane (Fig. 3B(d–f)).[60] The study highlighted that elastic constraints imposed by the SSE can generate sufficient loads leading to a complete blocking of the nucleation and growth of the dendrites, or altering the propagation direction and tortuosity.[60] AFM is also used in order to link the mechanism of heterogeneous dendritic growth to the morphological defects of LLZO during metal plating/stripping in an anode-free configuration.[61] As shown in Fig. 3C, continued Li-metal deposition led to a significant increase in surface roughness on the silver current collector. During the subsequent stripping process, the surface topography changed drastically compared to the initial state. This study further showed that Li-metal tends to deposit preferentially on surface defects of LLZO, such as scratches and pores. This behavior increases plating/stripping heterogeneity and accelerates short-circuit formation.

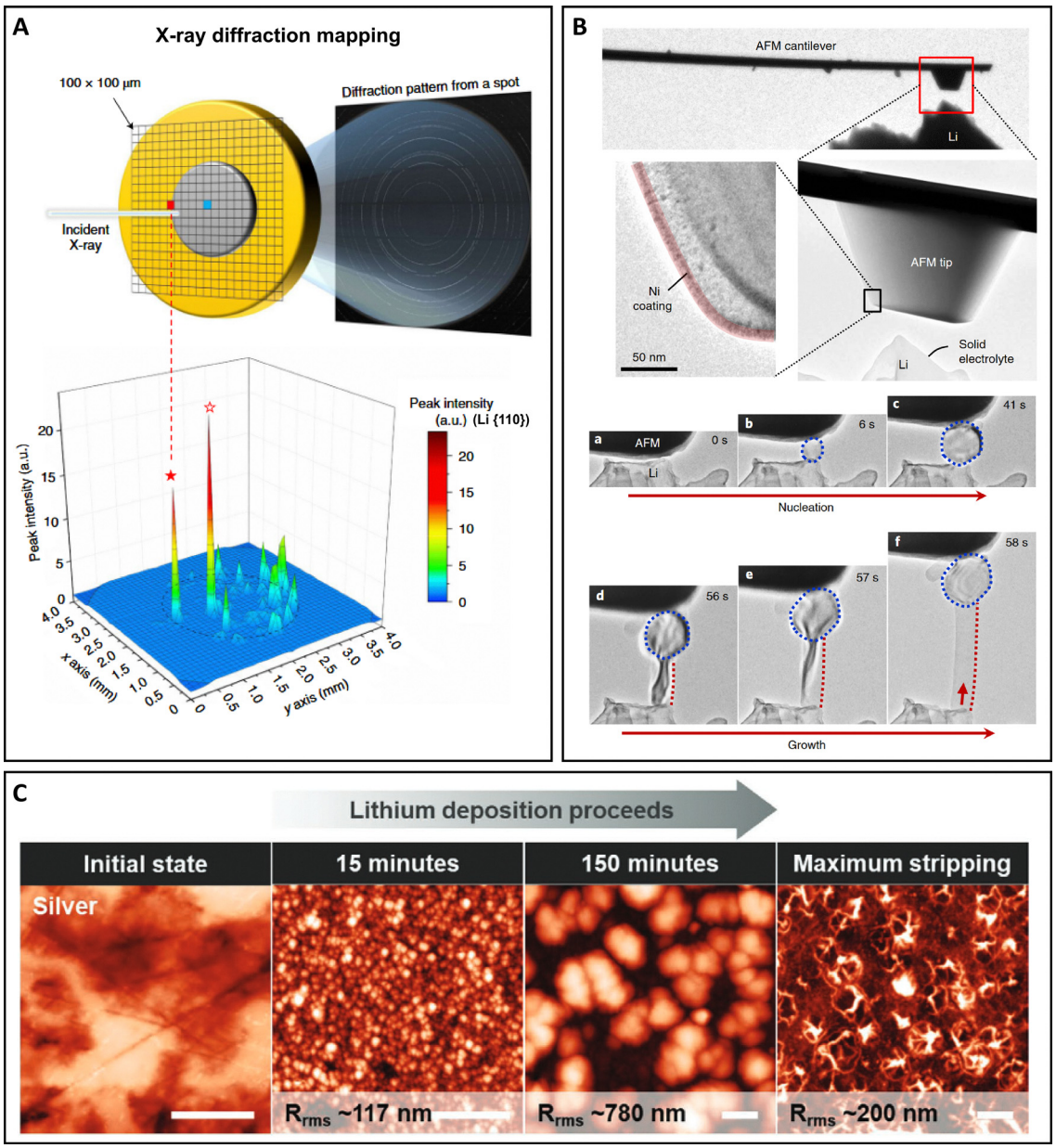

Fig. 3 Dendrite formation in an anode/SSE interface. (A) Illustration of spatially resolved X-ray diffraction (XRD) mapping and diffraction intensity of the Li-metal {110} peak, mapped across the sample to reveal the spatial distribution of Li-metal dendrites. Adapted with permission from ref. 57, Copyright 2021 Springer Nature. (B) TEM images of an *in situ* cell setup show Li-metal deposition through a native Li_2O solid electrolyte onto a Ni-coated, negatively biased AFM tip. A Li whisker forms and deflects the AFM cantilever upwards, until the compressive force increases, causing the whisker to buckle and collapse. Adapted with permission from ref. 60, Copyright 2019 Springer Nature. (C) AFM images of the surface of a silver interlayer at different charge/discharge states following galvanostatic Li-metal deposition at 0.2 mA cm^{-2} and stripping at 0.1 mA cm^{-2}. The scale bar for every image is 10 μm and R_{rms} is the root mean square roughness. Adapted with permission from ref. 61, Copyright 2020 Wiley-VCH Verlag Gmbh & Co. KGaA.

4.2.2. SEI formation. The formation of a SEI at the Li/SSE interface is one of the most prevalent buried degradation processes. It occurs at the micro- and nanoscale and has a significant impact on battery performance and lifetime.[59] X-ray tomography stands out as one of the most versatile techniques for probing buried characteristics of SSB materials, including SEI formation, detection of voids, and the assessment of the mechanical integrity *via* 3D reconstruction of material structures with nanoscale spatial resolution.[59,62,63] These capabilities are particularly valuable, as mechanical disintegration often occurs alongside SEI formation and dendrite growth.[59,64] In a study by Lewis *et al.*,[59] *operando* synchrotron X-ray tomography with a monochromatic beam was utilized to investigate the temporal evolution of the $Li/Li_{10}SnP_2S_{12}$ interface as displayed in Fig. 4A. This technique was combined with galvanostatic cycling of $Li/Li_{10}SnP_2S_{12}/Li$ symmetrical cells and tomography scans conducted at fixed 15-minute intervals.[59] The study successfully demonstrated the possibility of resolving

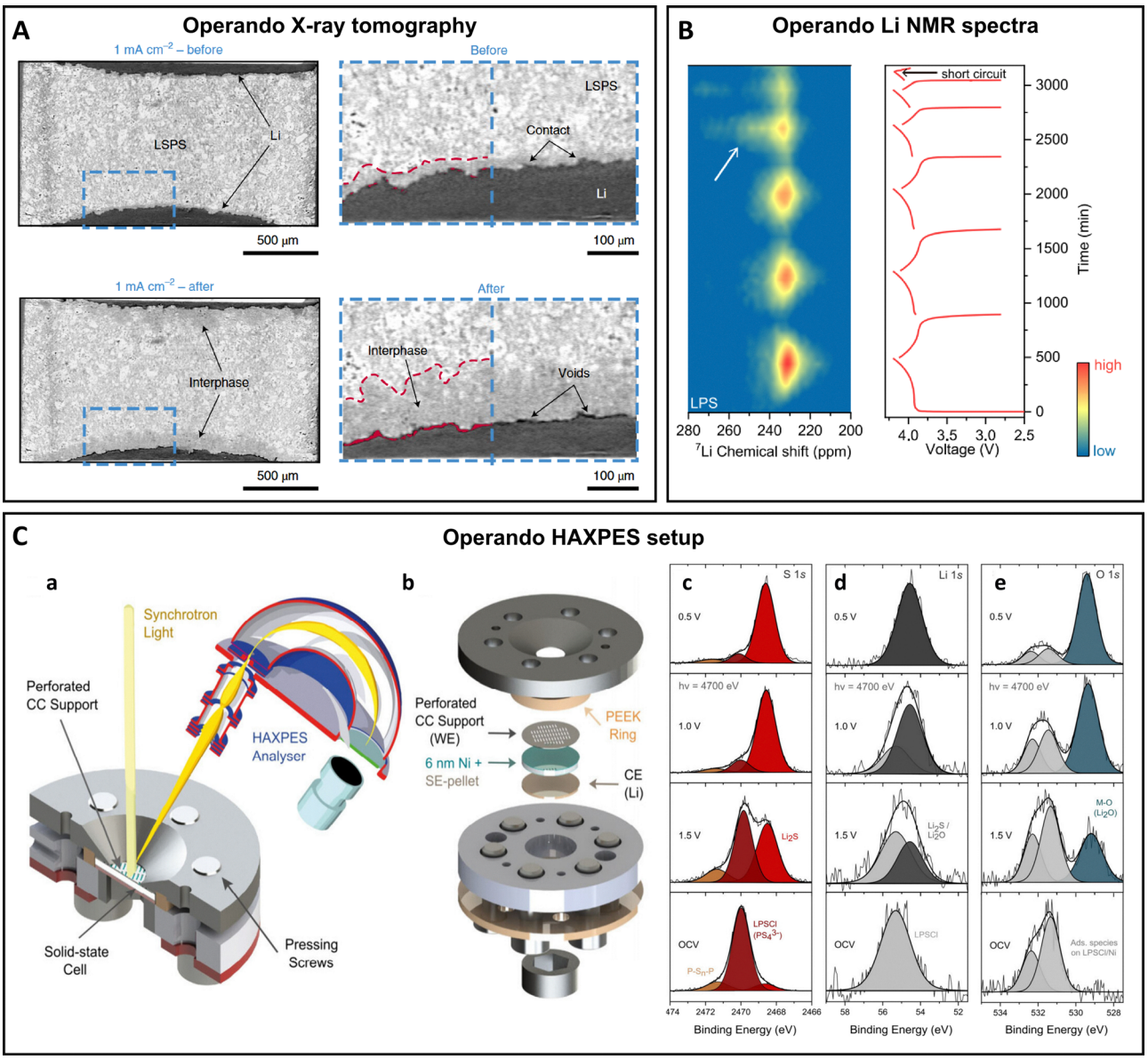

Fig. 4 SEI formation in an anode/SSE interface. (A) Cross-sectional images obtained from 3D tomographic datasets showing Li-metal electrodes (dark grey) and $Li_{10}SnP_2S_{12}$ (LSPS) electrolyte (light grey). Significant morphological changes and an increased volume of voids at the Li/LSPS interface following cycling at 1 mA cm^{-2} can be observed. Adapted with permission from ref. 59, Copyright 2021 Springer Nature. (B) Contour plots of ^7Li NMR spectra during cycling, shown alongside the charge/discharge profiles of anode-free SSBs employing $Li_7P_3S_{11}$ (LPS) as SSE. The ^7Li chemical shift signal at around 230 ppm is attributed to both active and inactive Li-metal plating. Adapted with permission from ref. 65, Copyright 2023 Springer Nature. (C) (a) Diagram illustrating the *operando* HAXPES setup. (b) Detailed schematic of the cell used for *operando* measurements. (c) S 1s, (d) Li 1s and (e) O 1s HAXPES spectra were acquired at an excitation energy of 4700 eV using the *operando* cell. The spectra compare measurements taken on the pristine Li_6PS_5Cl at open circuit voltage (OCV) and after formation of SEI by polarizing the cell at reduced potentials. Adapted with permission from ref. 67, Copyright 2024 American Chemical Society.

interfacial pores as well as SEI formation at the Li/$Li_{10}SnP_2S_{12}$ interface using the local Li concentration as the source of contrast. This achievement was attributed to the use of a monochromatic beam source which offers enhanced sensitivity to X-ray absorption.[59] During the Li-metal stripping, interfacial pore formation was the dominant process at the interface. Conversely, during the reduction step, the formation of a Li-rich SEI was observed instead of the expected metal plating. Fig. 4A demonstrates this by the cross-sectional images obtained from 3D tomographic datasets, which are recorded before and after cycling symmetrical cells at 1 mA cm^{-2}. The increased Li content in this SEI layer, possibly comprising Li_2S, Li_3P and Li–Sn alloys, created a contrast by reducing the average atomic number compared to $Li_{10}SnP_2S_{12}$.[59] Excess Li content within the SEI caused the interfacial layer to expand and irreversibly consume the Li-metal electrode through secondary chemical reactions.[59] Such a behavior indicated that short-circuiting due to dendrite growth is not the primary cause

of failure in the Li/$Li_{10}SnP_2S_{12}$ system. Instead, degradation is primarily driven by parasitic capacity loss due to the consumption of anode active materials during the SEI formation.[59] Furthermore, the SEI formation was linked to volume expansion, which induced compressive stresses that helped close the voids formed during the stripping process.[59]

Other techniques such as *operando* nuclear magnetic resonance (NMR) were utilized in a study by Liang *et al.*[65] to understand the mechanisms behind capacity loss and SEI formation. Their study focused on the interface between the *in situ* formed Li-metal and sulfide-based SSEs in an anode-free cell configuration.[65] The ^{7}Li chemical shift signal at 230 ppm in the NMR spectra was used as a quantitative indicator of Li-metal plating. As demonstrated in Fig. 4B, this signal increases during charge and disappears during discharge, indicating the deposition and stripping of Li-metal on the copper current collector, respectively. However, after multiple cycles, the signal no longer fully disappears during discharge. This suggests that a portion of the plated Li-metal cannot be stripped and is therefore considered inactive dead Li-metal. At the same time, the battery's capacity decreased with repeated cycling, which is reflected in a weaker signal during charging as well. The capacity fade in sulfide-based SSEs such as $Li_{10}GeP_2S_{12}$, $Li_{9.54}Si_{1.74}P_{1.44}S_{11.7}Cl_{0.3}$, Li_6PS_5Cl, and $Li_7P_3S_{11}$ was attributed to the cumulative effect of SEI formation and dead Li–metal plating. To disentangle the contributions of these processes, the authors used NMR signal integration to quantify dead Li–metal accumulation (as described above) and compared this with the overall discharge capacity loss. By assuming that total capacity loss reflects the combined effect of both mechanisms, nearly all the capacity loss was attributed to SEI formation in $Li_{10}GeP_2S_{12}$, indicating poor interfacial stability with Li-metal. In contrast, dead Li-metal deposition also played a significant role in performance degradation for other investigated sulfide SSEs (Fig. 4B). Furthermore, it was noted that in $Li_{10}GeP_2S_{12}$, Li-metal plating occurred prior to SEI formation and proceeded with very fast kinetics. This observation differs from a study reported by Morey *et al.*,[66] where the initial degradation was attributed to direct reduction of the SSE during the charging process. Here, a Li_6PS_5Cl pellet was placed on top of a Li-metal foil inside an Ar-filled glovebox. The resulting stack was mounted on a sample holder, which was then transferred to Auger and X-ray photoelectron spectroscopy (XPS) instruments in a protective environment. The exposed surface of the Li_6PS_5Cl pellet was irradiated with an electron beam to accumulate negative charge, while the Li-metal electrode foil was grounded.[66] This created a potential difference across the SSE pellet, enabling Li-metal plating on the exposed surface. This configuration allowed for *in situ* Auger and XPS measurements to investigate interfacial processes such as SEI formation and Li-metal plating, without the need for electrical contacts to the cell. Both Auger and XPS spectra revealed that the SEI formation occurred *via* direct reduction of Li_6PS_5Cl to compounds such as Li_2S and LiCl. This SEI formation was subsequently followed by Li-metal plating on top of the SEI layer,[66] further confirming the correlated occurrence of these two phenomena during charge.[66] Additionally, the study noted that due to the longer acquisition time required for XPS compared to Auger spectroscopy, some of the porous plated Li-metal underwent slow oxidation to Li_2O, attributed to the residual oxygen partial pressure (9×10^{-9} mbar) in the chamber.[66]

In a study by Aktekin *et al.*,[67] *operando* hard X-ray photoelectron spectroscopy (HAXPES) was employed to understand the mechanism of Li_6PS_5Cl electrochemical decomposition in contact with Li-metal and subsequent SEI formation. As shown in Fig. 4C(a and b), a 6 nm thin film of Ni was deposited on the surface of the SSE to serve as the working electrode.[67] A Li-metal foil counter electrode was placed on the opposite side of the SSE. The assembled cell was housed in a chamber typically used for *operando* optical imaging.[68] High-energy photons from a synchrotron source were directed at the Ni-coated side of the SSE. This X-ray source, with a photon energy of 4700 eV, enabled the acquisition of XPS spectra from the SSE/Ni interface buried 6 nm below the surface. By polarizing the Ni working electrode from its open circuit condition (1.94 V *vs.* Li^+/Li) to more reducing potentials in the range of 1.5–0.5 V, the authors could clearly detect the appearance of new peaks in S 1s, Li 1s and O 1s HAXPES spectra (Fig. 4C(c–e)).[67] These new peaks were attributed to decomposition of Li_6PS_5Cl into Li_2S and Li_2O. Furthermore, the study demonstrated that a significant portion of the SEI could be oxidized to form sulfite, sulfate, and polysulfide species at high oxidation potentials up to 4 V. Importantly, this SEI formation/reoxidation process was shown to be electrochemically reversible and compounds within the SEI could be regenerated upon reducing the working electrode during Li-metal plating.[67]

As demonstrated in many of the studies discussed here, stabilizing the SSE against Li-metal and minimizing the formation of an SEI is a crucial strategy for improving the cycling lifetime of SSBs. One of the most effective ways to enhance the interfacial stability between the Li-metal and SSE is the introduction of artificial metal interlayers, such as Ag and Au, between these two components.[69] These interlayers not only protect the SSE from undesirable chemical reactions but also promote more uniform plating and stripping cycles by alloying with Li-metal.[69] However, these alloys are highly unstable under ambient conditions, making them difficult to characterize *ex situ*. Yun *et al.*[69] addressed this challenge by developing an *operando* XPS technique to investigate these interlayers during SSB cycling. For their study, the XPS sample holder was modified with two electrode contacts allowing the LLZO SSE to be sandwiched between a Li-metal counter electrode and a metal interlayer serving as the working electrode. The entire assembly was carried out inside a glovebox, and the sample holder was transferred to the XPS chamber under vacuum.[69] The XPS measurements were performed under ultra-high vacuum while the cell was actively cycling. The *operando* observation of Li-metal plating/stripping was demonstrated based on the temporal tracking of Li-metal and Ag peaks in the XPS spectra. In addition to revealing the plating/stripping behavior, the XPS data also indicated the progressive formation of Li_2O during cycling. These effects were attributed to residual

contaminants such as carbonates and metal oxides on the LLZO and Ag surfaces.[69] This ongoing oxidation represents an undesirable SEI formation, which contributes to increased interfacial resistance and capacity loss by converting active Li–alloy into electrochemically inactive oxide compounds, as shown in the previously discussed studies.

As mentioned in Section 4.1.2, solid polymer electrolytes are recently receiving attention as an alternative to inorganic SSEs owing to their flexibility, ease of manufacturing, good interfacial contact, and cost efficiency.[70–72] However, these solid organic electrolytes face a set of key challenges, including low ionic conductivity and severe chemical reactivity with Li-metal anodes resulting in undesired SEI formation.[70–72] The enhancement of the interfacial properties of the Li-metal/organic-polymer–electrolyte interface and the role of Li_2S additives were explored in a study by Sheng *et al.*[72] In this work, cryo-TEM was employed to protect the Li-metal/PEO interface from damage that would typically occur under standard TEM conditions due to the high reactivity of the Li-metal. The study captured nanoscale details of the Li-metal/PEO interface, particularly the formation of LiF nanocrystals at this boundary. These nanoparticles originated from the accelerated decomposition of lithium bis(trifluoromethanesulfonyl)imide (LiTFSI) salt within PEO in contact with Li-metal, due to addition of the Li_2S additive. Importantly, they were shown to play a crucial role in enhancing interfacial stability by preventing further reactions between the PEO and Li-metal.[72]

4.2.3. Lithiation induced heterogeneities. Although SSBs are typically associated with the use of Li-metal as an anode, other types of active materials based on intercalation and alloying are also used. Visualization of the lithiation process in anode materials such as silicon, graphite, and LTO is crucial for understanding how volume changes, interfacial evolution, and phase transformations contribute to degradation phenomena in SSBs. This subsection highlights key imaging methodologies used to study lithiation in these materials and their relevance to performance-limiting mechanisms.

Carbon allotropes with the capability of reversible intercalation/deintercalation of Li^+ have played a special role in battery development.[73] The use of graphite as an anode material was a key factor in the commercial success of LIBs more than 30 years ago due to its long cycling stability and favorable energy density.[74] Considering the light weight of Li^+ and the susceptibility of carbon allotropes to knock on damage by electron beam irradiation, imaging the process of Li^+ uptake in this category of anode materials is challenging and usually requires special measures.[73] In order to address this challenge and protect the samples from beam damage, Kuhne *et al.*[73] employed a low voltage TEM setup with electrons accelerated by a voltage of 80 kV. This strategy has previously been used for imaging thick sections (100 nm or above) of organic materials.[75] Furthermore, spherical and chromatic aberration corrections were utilized to enhance contrast and resolution. This study considered an electrochemical cell with two electrodes comprising Si_3N_4/graphene and Si_3N_4 as well as a solid polymer electrolyte applied with a drop casting technique (Fig. 5A).[73] LiTFSI salt was added to the electrolyte to provide ionic conductivity and act as a Li^+ source. Although an organic solid polymer electrolyte was utilized in this study, the methodology and results translate to SSBs as well. The bilayer graphene was positioned partially on a hole in the substrate for electron imaging and EELS data acquisition during the intercalation.[73] The study demonstrated that the intercalated Li^+ arrange themselves in a multi-layered close-packed structure between the graphene sheets. This arrangement allows for a much higher charge storage capacity than the densest known configuration in bulk graphite (LiC_6). The findings suggest that two-dimensional materials like bilayer graphene can host unique ion storage arrangements that differ from those in their bulk counterparts.[73] In a similar study, the change in spacing between graphene layers, during intercalation of PF_6^-, and the consequent mechanical deformations were characterized using *in situ* AFM, pointing towards the possibility of using similar setups for investigation of lithiation phenomena.[76]

High-capacity materials often undergo significant volumetric changes during cycling, leading to mechanical detachment and microcracking.[77] As an example, the anisotropic swelling of silicon active materials, such as nanowires with volume expansions up to 300% during lithiation, has been successfully imaged using TEM.[78] This extreme anisotropic swelling is particularly important in graphite–silicon composite electrodes since it can cause detachment of silicon active material particles from the electronically conductive graphite network, and hence disrupt the electron percolation required for continued lithiation.[77] Therefore, the mechanical stabilization of micrometer-sized active particles by a carbon black-binder network is crucial to maintain electrochemical activity in silicon anodes.[77] It was demonstrated that the mechanical disintegration induced by swelling, alongside continuous SEI growth on silicon particles, are the major contributors to the capacity fade.[77] Imaging and quantifying the detachment of the carbon black-binder domain from active particles is a significant challenge due to the need for precise multi-phase segmentation.[77] Effective analysis requires distinguishing at least five phases: pore space, silicon particles, graphite particles, the carbon black-binder domain, and the SEI layer.[77] The primary difficulties arise from the need for high-spatial resolution to capture the nanometer-sized features of the carbon black-binder domain and the weak imaging signal from light elements, which results in poor contrast against graphite particles in attenuation-based X-ray and electron backscatter imaging.[77] A study by Muller *et al.*[77] (Fig. 5B) focused on visualizing and quantifying such detachment using transmission X-ray tomographic microscopy (TXTM) and developing a model to describe the interplay between the mechanical and electrochemical dynamics. In this study, a specific approach was employed which involved replacing 50 vol% of the carbon-black with carbon-coated copper nanoparticles.[77] Copper nanoparticles enhance contrast due to their heavier atomic weight and maintain electrical conductivity comparable to carbon-black. Furthermore, copper is stable under electrochemical conditions and does not interfere with the electrochemical

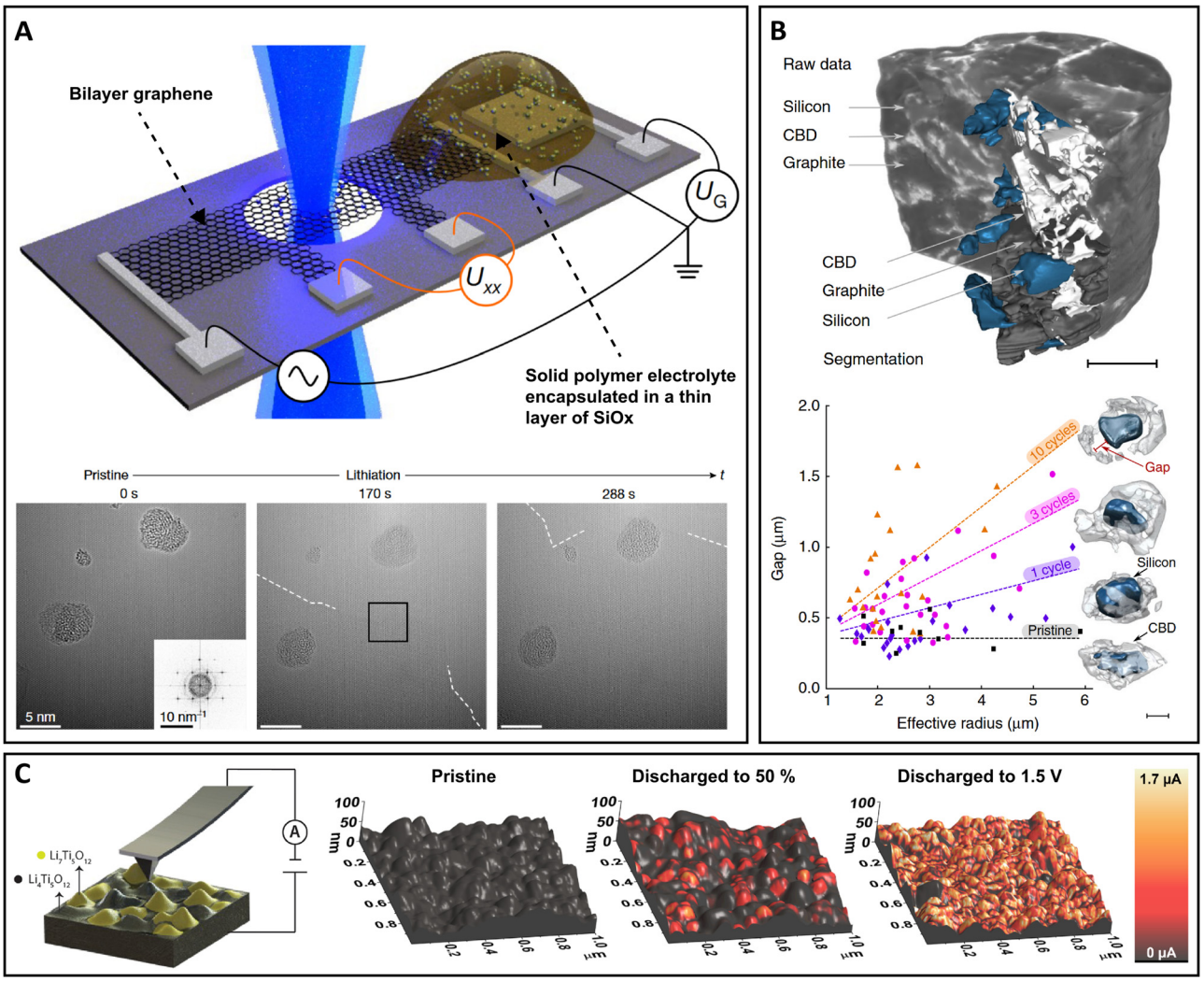

Fig. 5 Lithiation induced heterogeneities. (A) Schematic representation of a cell setup designed for *in situ* TEM analysis. The cell consists of a bilayer graphene which is partially suspended over a hole in the Si_3N_4-covered Si substrate, as well as a solid polymer electrolyte which is connected to a metallic counter electrode. The image below shows the results of the TEM measurements, illustrating a Li-crystal developing within the bilayer graphene during the lithiation process. Adapted with permission from ref. 73, Copyright 2018 Springer Nature. (B) Raw TXTM data of a pristine silicon–graphite electrode with multi-phase segmentation, highlighting silicon (blue), graphite (dark grey), carbon black-binder (light gray), and pore spaces. Scale bar: 15 µm. The image below displays the average gap between the silicon particle surfaces and the carbon black-binder domains as a function of particle radius and cycle number. Scale bar: 5 µm. Adapted with permission from ref. 77, Copyright 2018 Springer Nature. (C) Schematic showcasing how conductive atomic force microscopy (c-AFM) can identify the presence of different phases based on their distinct conductivity properties. 3D topographical c-AFM images of lithium titanate (LTO) thin-films are presented at various charge states: pristine, 50% discharged, and discharged to 1.5 V. The color gradient reflects the measured current, as shown by the accompanying scale bar. Adapted with permission from ref. 30, Copyright 2016 American Chemical Society.

performance of the cell.[77] The data were acquired on pristine and cycled electrodes using samples that were vacuum-infiltrated with epoxy resin for mechanical stability.[77] The setup, including a fast laser-milling apparatus to prepare samples with a 50 µm diameter, achieves a voxel size of approximately 30 nm. This voxel-size enables high-resolution 3D visualization of electrode microstructures and detachment phenomena.[77] Fig. 5B displays a reconstructed tomogram of a pristine sample with a four-phase segmentation of silicon particles, graphite particles, the carbon-black-binder domains, and pores. By utilizing prior knowledge of the particle size and porosity, the weakly attenuating graphite particles were distinguished from the pore space. The segmented tomography data were used to evaluate the average distance between silicon particles and the nearest carbon-black-binder domain through a ray tracing approach. Fig. 5B illustrates that this gap distance increases with both the radius of the silicon particles and the number of cycles, with dotted lines providing a visual guide to these trends.

While silicon has been heavily pursued as a high-capacity anode material for advanced LIBs, intercalation oxide anodes such as $Li_4Ti_5O_{12}$ (LTO) are often considered inferior due to their lower capacity and higher voltage compared to graphite.[30] However, the high redox potential of LTO, which lies safely

within the electrolyte electrochemical stability window, allows for cycling this material without the formation of detrimental passivation layers. Furthermore, LTO belongs to the group of zero-strain electrodes, where the lithiation/delithiation does not result in any significant change in the volume of material.[79] Therefore, this material offers exceptional stability, robustness, and safety, which has led to its successful commercialization despite its lower energy density.[30] While LTO is valued for its stability and safety, the precise mechanism behind the phase transformation between $Li_4Ti_5O_{12}$ and $Li_7Ti_5O_{12}$ during charge/discharge remains unclear. This difficulty is due to the nearly identical lattice parameters of the two phases, which makes their separate identification very challenging using diffraction-based techniques.[30] A study by Verde *et al.*[30] leveraged the difference in electronic conductivity between the $Li_4Ti_5O_{12}$ and $Li_7Ti_5O_{12}$ phases and used c-AFM to directly visualize phase formation and distribution at the nanoscale. Upon discharging LTO to 50% capacity, the surface morphology remained largely unchanged, but the electronic conductivity increased significantly. Initially, no current was measured with c-AFM in the pristine LTO, but current was detected within individual grains after discharging to 50% capacity, averaging 0.12 μA μm^{-2} (Fig. 5C).[30] This current increased to 0.58 μA μm^{-2} after further discharge to 1.5 V, which marks the end of the discharge plateau and an almost fully discharged state. This indicated that nearly all grains in the LTO film became electronically conductive following the completion of the two-phase reaction.[30] The current was localized within discrete grains, suggesting that the $Li_4Ti_5O_{12}$ to $Li_7Ti_5O_{12}$ phase transition occurs through narrow percolation channels rather than propagating laterally across grains. The current images revealed well-defined particles with no current at the grain boundaries, suggesting that the phase transition is limited to specific structural environments.[30]

4.3. Cathodes

As shown in Fig. 1, the main degradation mechanisms at the cathode/SSE interface in SSBs include the formation of undesired CEI phases and the loss of contact between the electron/ion-conducting network and the CAMs. This section reviews recent studies that employ micro- and nanoscale characterization techniques to investigate these degradation pathways. Furthermore, it examines research works focused on state-of-charge mapping and heterogeneous lithiation within the CAM particles.

4.3.1. CEI formation. The cathode/SSE interfaces in SSBs play a crucial role in determining the overall battery performance, as they significantly impact the charge transfer resistance.[80] Characterizing this interface with high spatial resolution is essential for understanding degradation mechanisms affecting cathode performance. For instance, TEM-based techniques are invaluable in these types of studies, since they offer nanoscale insights into both structural and compositional aspects of the cathode/SSE interface. Vardar *et al.*[80] investigated the structural and chemical evolution of the Li_xCoO_2(LCO)/LLZO interface as a function of annealing temperature. In Fig. 6A, TEM images of the LCO/LLZO interface highlighted notable morphological transformations, where the initially continuous interface exhibited increased porosity after annealing at 500 °C. This change was accompanied by the emergence of nanocrystalline LCO and formation of a CEI, which is further confirmed by selected area electron diffraction. The study identified significant interdiffusion of cations across the interface using energy-dispersive X-ray spectroscopy (EDX) analysis. This interdiffusion and associated CEI formation resulted in an expansion of the interface width after annealing. Moreover, voids were also observed at this interface, likely resulting from the formation of Li_2CO_3 on the LCO surface due to exposure to CO_2 in air. During the annealing process, Li_2CO_3 decomposed, leaving behind voids. This phenomenon further weakened the contact between the phases at the cathode/SSE interface. Using a range of complementary characterization techniques, including XPS, secondary ion mass spectroscopy (SIMS), synchrotron XRD and absorption spectroscopy, the study revealed that cation interdiffusion and secondary phase formation, such as $La_2Zr_2O_7$ and Li_2CO_3, begin at temperatures as low as 300 °C.[80] Further heat treatment at higher temperatures such as 500 °C leads to significant degradation of the electrochemical performance with an eightfold increase in the charge transfer resistance.[80] To minimize adverse reactions and reduce interfacial resistance, it was recommended to employ processing at lower temperatures and shorter annealing durations in environments free of CO_2. Similar interfaces, $Li_{6.75}La_{2.84}Y_{0.16}Zr_{1.75}Ta_{0.25}O_{12}$/LCO in particular, were also investigated using *in situ* TEM to directly image the temporal evolution of the CEI during Li^+ uptake.[81]

In another study displayed in Fig. 6B, Wang *et al.*[82] focused on the interfacial chemical and electrochemical reactions in a sulfide-based SSE system. The emphasis was on the formation of a CEI at the interface between a sulfide electrolyte and a single-crystal layered oxide cathode. $Li_{10}GeP_2S_{12}$ with its very high ionic conductivity was chosen as the SSE, while single-crystal $LiNi_{0.5}Mn_{0.3}Co_{0.2}O_2$ (NMC532) was selected as the cathode due to its cycling stability and resistance to particle cracking.[82] To enhance interfacial stability, a 10 nm $LiNb_{0.5}Ta_{0.5}O_3$ (LNTO) coating was applied to the NMC532 surface, as confirmed by scanning TEM (STEM) coupled with EDX analysis.[82] STEM-EDX was employed in this work to map the elemental distribution of Ni, Co, Mn, O, Nb, and Ta. The results validated the homogeneity of the materials at the nanoscale (Fig. 6B(a–e)) and confirmed the uniform coating of LNTO on the NMC532 surface (Fig. 6B(f–l)).[82] The study further highlighted the challenges of large interfacial resistance arising from oxygen loss at the cathode/SSE interface. This oxygen loss from the cathode side led to the chemical oxidation of $Li_{10}GeP_2S_{12}$ and the formation of a CEI comprising oxygen-containing species like phosphates, sulfates, and sulfites. A detrimental structural transformation to a rock-salt phase in the oxide cathode was also induced by this phenomenon. Additionally, the authors demonstrated that the high operating voltages resulted in electrochemical generation of interfacial species that do not contain oxygen such as polysulfides. The

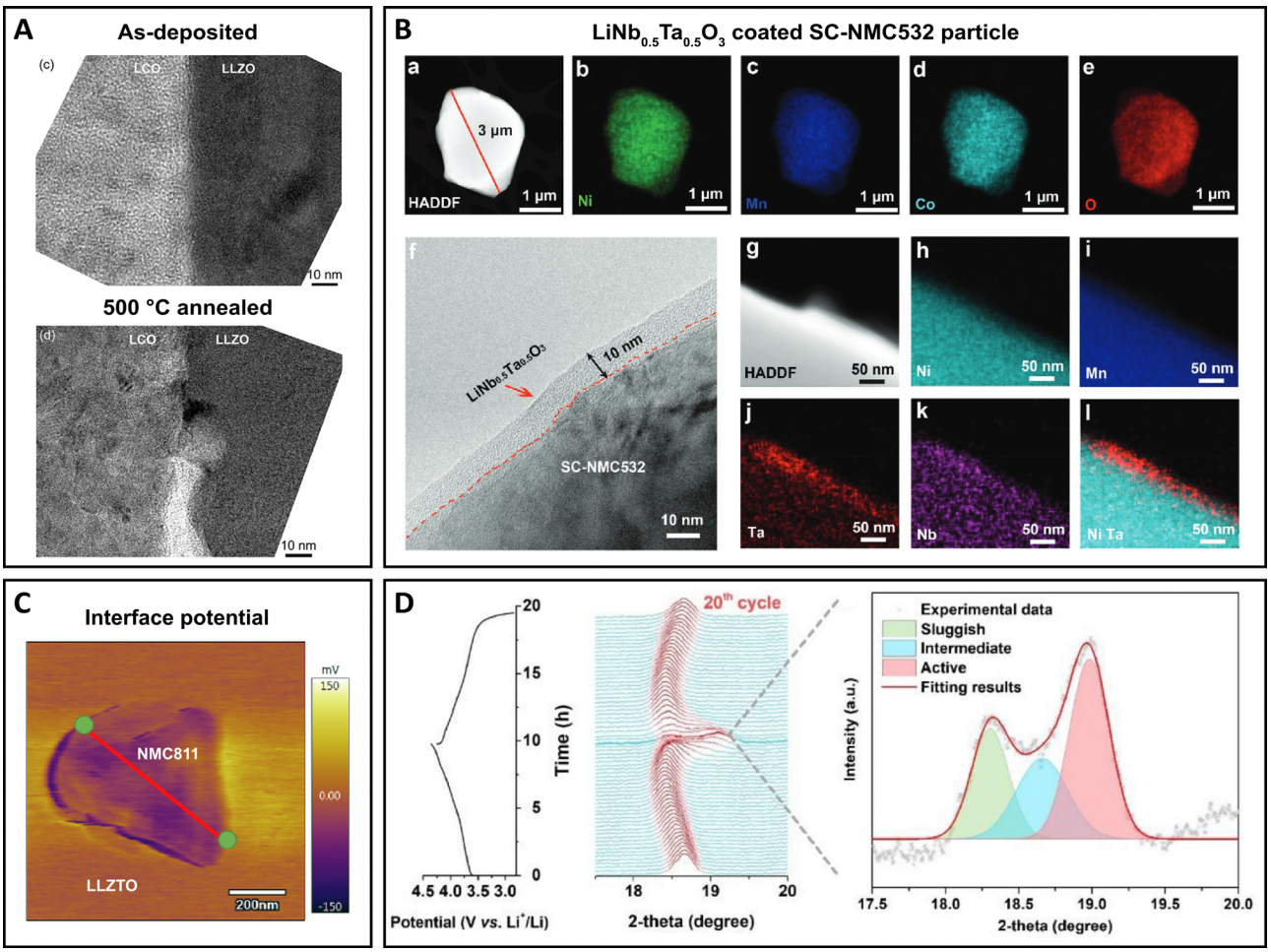

Fig. 6 Cathode CEI formation. (A) TEM bright field image of the interface between LCO and LLZO, both in the as-deposited state and following annealing at 500 °C. Adapted with permission from ref. 80, Copyright 2018 American Chemical Society. (B) High-resolution TEM images showing pristine and coated single-crystal (SC)-NMC532 samples. (a) High-angle annular dark-field (HAADF) image of SC-NMC532. (b)–(e) Elemental maps of Ni, Mn, Co, and O for SC-NMC532 captured using STEM-EDX. (f) Bright-field TEM image of a LNTO coating on SC-NMC532. (g) HAADF image of LNTO coating on SC-NMC532. (h)–(k) Elemental maps of Ni, Mn, Ta, and Nb for LNTO coating using STEM-EDX. (l) Combined Ni and Ta elemental map of LNTO coating on SC-NMC532. Adapted with permission from ref. 82, Copyright 2021 Wiley-VCH Verlag Gmbh & Co. KGaA. (C) AFM image showing the interface potential of NMC811 and LLZTO. Adapted with permission from ref. 84, Copyright 2021 Elsevier. (D) Structural characterization of an NMC811 electrode in an all-solid-state battery (ASSB). *Operando* XRD patterns showing the extracted (003) reflections of the NMC811 electrode at the 20th cycle. The (003) reflections at 4.35 V were fitted and associated with the sluggish, intermediate, and active phases of NMC811. Adapted with permission from ref. 85, Copyright 2023 Elsevier.

interfacial coating of LNTO on the cathode was shown to mitigate the chemically induced interfacial degradation but it could not prevent undesired electrochemical reactions.[82]

Additional critical insights into how these interfacial dynamics can hinder battery efficiency and lifespan were gained by Wang *et al.*[83] using *in situ* STEM paired with EELS. An LCO/lithium phosphorous oxynitride (LiPON) interface was examined in this work within a thin-film battery setup. The characterization revealed a structurally disordered CEI layer at the boundary between the cathode and SSE.[83] This layer chemically formed during the fabrication and underwent further changes during the charging process, resulting in the formation of Li_2O and Li_2O_2 as well as an increased Co oxidation state in LCO. These changes were identified as the primary cause of irreversible capacity loss and increased interfacial impedance.[83]

SPM techniques also play a pivotal role in characterizing cathode/SSE interfaces by providing detailed insights into surface potentials, topography, and interfacial properties at the nanoscale. Zhao *et al.*[84] presented a strategy to enhance the interface properties between nickel-rich $LiNi_{0.8}Mn_{0.1}Co_{0.1}O_2$ (NMC811) cathodes and garnet-type SSE $Li_{6.4}La_3Zr_{1.4}Ta_{0.6}O_{12}$ (LLZTO) through interfacial engineering. By introducing a Li_3PO_4 layer *via* an *in situ* calcination process, a compatible Li^+-conductive interface was formed. The TEM with EDX analysis confirmed the formation of a 10 nm thick Li_3PO_4 layer on the NMC811 particles.[84] Scanning Kelvin probe microscopy (SKPM) was then used to analyze the surface potential of

NMC811–LLZTO and NMC811–Li_3PO_4–LLZTO cathodes as shown in Fig. 6C. This analysis revealed that the engineered interface significantly reduces the space charge layer effect in the NMC811–Li_3PO_4–LLZTO cathode.[84] The modified sample showed a lower potential drop, indicating better interface compatibility and enhanced electrochemical performance.[84] Furthermore, this engineered interface not only mitigated the formation of an insulating CEI but also significantly reduced interfacial impedance and improved Li^+ conductivity.[84] To further demonstrate the benefits of this surface modification, the authors investigated the resulting performance improvements in full battery cells. The NMC811/LLZTO/Li cell exhibited an initial discharge capacity of 175 mAh g^{-1} but only retained 20% of that capacity after 50 cycles at a 0.2C-rate. In contrast, the NMC811–Li_3PO_4–LLZTO/LLZTO/Li cell demonstrated an increased initial discharge capacity of 188.8 mAh g^{-1} with a capacity retention of 94% under similar cycling conditions.[84]

In another study, Liu *et al.*[85] employed *operando* XRD (Fig. 6D) to investigate bulk structural degradation of single-crystal NMC811 when in contact with the sulfide-based $Li_{10}SnP_2S_{12}$ SSE.[85] Their results revealed that even during the initial charge, NMC811 undergoes decomposition, forming both a non-layered rock-salt phase and an amorphous insulating CEI.[85] Interestingly, similar structural degradation has been observed in NMC-type materials used in conventional LIBs with liquid electrolytes.[86] However, in those systems, such decomposition typically occurs only after hundreds of cycles.[85] In contrast, the *operando* XRD data showed that in solid-state systems, degradation products begin forming early and continue to accumulate with cycling.[85] As shown in Fig. 6D multiple (003) reflections at 4.35 V were associated with sluggish, intermediate, and active phases of NMC811 after 20 cycles. The authors propose that quantifying these degradation phases could serve as a useful diagnostic tool for evaluating the impact of surface coatings or compositional modifications aimed at improving cathode performance in SSBs.[85]

Multi-scale, high-resolution X-ray spectroscopy techniques have also been employed to investigate the CEI formation. In a recent study, Lelotte *et al.*[87] utilized advanced techniques such as synchrotron-based X-ray absorption spectroscopy (XAS), X-ray photoemission electron microscopy (XPEEM), and XPS for high-resolution chemical imaging and elemental analysis of degradation products formed at the interface between $LiNi_{0.6}Co_{0.2}Mn_{0.2}O_2$ (NMC622) and Li_6PS_5Cl. To isolate the contribution of the SSE to CEI formation, independent of the cathode particles, the authors constructed a model cell with the configuration of $InLi_x$/Li_6PS_5Cl/Li_6PS_5Cl–carbon. Cyclic voltammetry was performed across a potential window similar to that experienced by the SSE when paired with NMC622. Under these conditions, Li_6PS_5Cl was found to undergo irreversible oxidation, highlighting its direct contribution to CEI formation through degradation products. Post-mortem XAS analysis revealed that the oxidized products were primarily confined to a thin nanoscale layer on the Li_6PS_5Cl surface. This reaction was also associated with volumetric shrinkage, potentially leading to contact loss from carbon additives, which was confirmed by monitoring pressure changes during oxidation. The findings demonstrate that, beyond structural degradation of NMC (*e.g.*, oxygen release and rock-salt phase formation), the SSE itself plays a significant role in CEI formation. The oxidation of Li_6PS_5Cl in the vicinity of LCO is also reported in other studies,[88] in which they used *operando* XPS for recording the temporal evolution of the CEI.

4.3.2. Contact loss and heterogeneous lithiation. Like Si-based anodes, intercalation-based CAMs also undergo volume changes during charge/discharge cycles. However, these volume changes are relatively smaller and typically lead to minor cracking.[89] Still, as mentioned earlier, the cathode layer in SSBs is a composite consisting of a SSE, an electronically conducting carbon matrix and CAM particles. As a result, even minor cracks often manifest as contact loss between the CAM particles and the conductive network (typically the SSE particles) after multiple cycles.[89,90] One direct effect of contact loss is that the disconnected regions of the CAM particles become inactive in the lithiation reaction. This phenomenon leads to a more rapid capacity fade in SSBs in comparison to the LIBs using liquid electrolytes.[90] Shi *et al.*[90] investigated this type of degradation in a composite cathode layer composed of NMC532, amorphous $75Li_2S$–$25P_2S_5$ SSE particles and carbon nanofibers using nanoscale FIB–SEM tomography. Furthermore, the NMC532 particles were coated with an amorphous Li–Zr–oxide layer to enhance their chemical stability when in contact with the SSE. This coating also ensured that the chemical degradation did not contribute to mechanical disintegration, allowing the study to attribute contact loss solely to the shrinkage and expansion of the CAM during cycling.[90] After an initial linear capacity fade from 140 mAh g^{-1} to 100 mAh g^{-1}, a sharp drop was observed between 30th and 40th cycles, with the capacity falling below 20 mAh g^{-1}. The authors attributed this significant capacity fade primarily to mechanical degradation phenomena, such as contact loss, rather than chemical incompatibility. This conclusion was supported by the recovery of capacity to 80 mAh g^{-1} after applying 300 MPa of pressure to the degraded cell. To directly observe the evolution of contact loss during cycling, cells in the discharged state were investigated. An area of interest on the cathode was marked by ion-milling trenches around it, and its cross-section was exposed for SEM imaging. A 2D backscattered SEM image was first captured from the cross-section, after which a 50 nm slice was milled away and another 2D image was recorded. This process was repeated hundreds of times, and the resulting 2D images were then combined and reconstructed into a 3D volume (Fig. 7A(a–c)). As shown in Fig. 7A(d), the cathode composite initially contained approximately 3 vol% of voids before cycling, and this void volume remained largely unchanged after 10 cycles (Fig. 7A(e)). However, after 50 cycles, the void volume increased threefold to nearly 10 vol% (Fig. 7A(f)), supporting the hypothesis that the observed capacity fade results from contact loss.[90]

Lou *et al.*[91] also investigated the interfacial dynamics and local Li^+ transport in polycrystalline cathodes utilizing synchrotron transmission X-ray microscopy (TXM). The nanoscale 3D

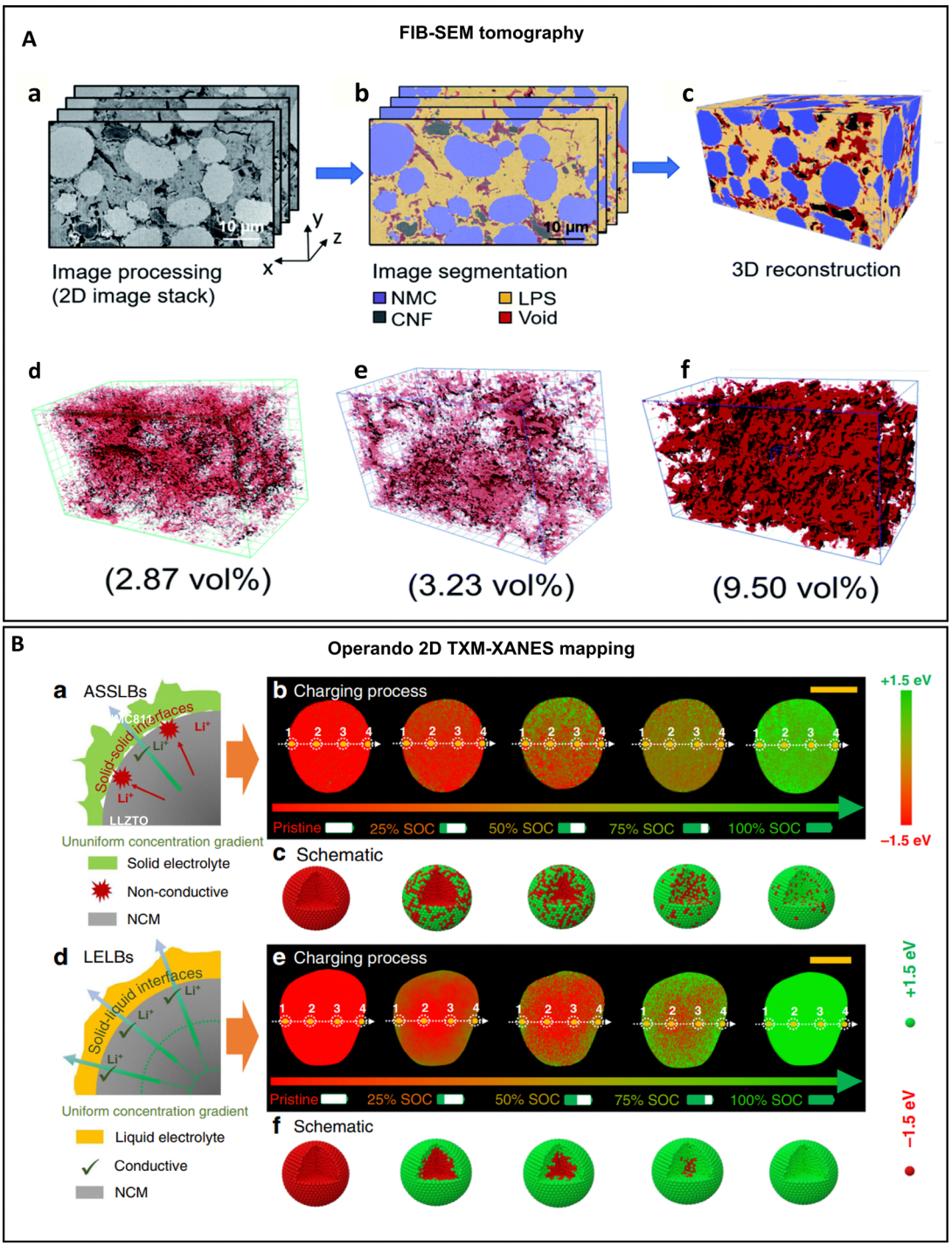

Fig. 7 Contact loss and microcracking (A) FIB–SEM tomography conducted on a cathode composite layer of NMC532, $75Li_2S–25P_2S_5$ (LPS in the figure) and carbon nanofibers (CNF) demonstrating (a) stack of 2D images obtained from multiple cycles of FIB milling and SEM imaging in backscattered electron mode, (b) four-phase segmentation of acquired stack of 2D images and (c) 3D reconstruction of the composite layer volume. Adapted with permission from ref. 90, Copyright 2020 Royal Society of Chemistry. (B) Combined 2D TXM-XANES mapping and X-ray nanotomography: (a) schematic representation of solid–solid interface models and kinetics. (b) TXM-XANES mapping of a single cathode particle of NMC622 during charging in a SSB, with (c) a corresponding schematic of the heterogeneous charging process of an NMC622 particle. (d) Schematic of solid–liquid interface models and kinetics, (e) TXM-XANES mapping of a single cathode particle of NMC622 during charging in a liquid electrolyte, and (f) a schematic illustrating the homogenous charging process of an NMC622 particle in a LIB using liquid electrolyte. Scale bar: 10 μm. Adapted with permission from ref. 91, Copyright 2020 Springer Nature.

rendering reconstructed from X-ray tomography showed that a significant number of microcracks develop in the NMC622 particles after 50 cycles with solid/solid interfaces in SSBs, causing interfacial contact loss, phase heterogeneity, and eventual particle degradation (see schematics in Fig. 7B(a)).[91] In contrast, no microcracks and contact loss were observed in the

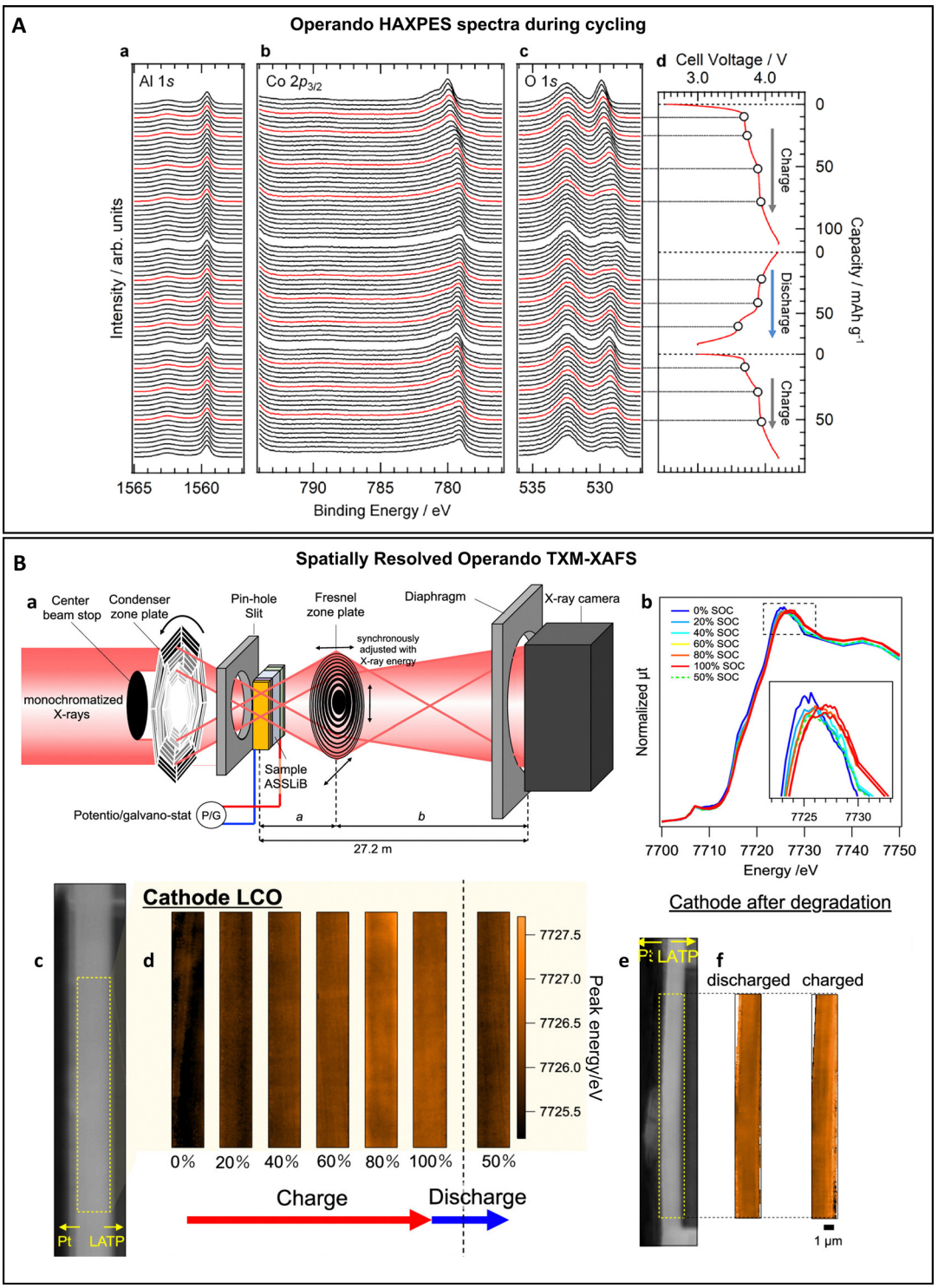

Fig. 8 Cycling-induced heterogeneities in cathode (A) *operando* HAXPES spectra of (a) Al 1s, (b) Co $2p_{3/2}$, and (c) O 1s recorded at different states-of-charge (SOC) during the first charge/discharge cycle of a thin-film LCO cathode layer, and (d) corresponding charge/discharge curve of a thin-film SSB cell during *operando* HAXPES. Adapted with permission from ref. 93, Copyright 2020 Elsevier. (B) Spatially resolved *operando* TXM-XAFS on a thin-film LCO cathode layer, (a) Schematic of the TXM-XAFS setup, (b) XANES spectra of the thin-film LCO at different states-of-charge, (c) absorption image of a thin-film LCO layer in contact with SSE, (d) state-of-charge mapping of a thin-film LCO layer during first charge/discharge (brighter areas correspond to higher valence of Co and hence higher state-of-charge), (e) absorption image of degraded thin-film LCO demonstrating the contact loss from SSE after 100 charge/discharge cycles, and (f) state-of-charge mapping of a degraded thin-film LCO layer at fully charge and fully discharge states. Adapted with permission from ref. 94, Copyright 2023 American Chemical Society.

cycled electrodes of batteries with liquid electrolytes after 50 cycles.[91] *In operando* TXM-XANES was also used to investigate the relationship between the local interface environment and electrochemical properties. In this approach, tunable incident photon energy using XAS provided detailed information about the chemical state with a spatial resolution of around 30 nm.[91] By analyzing the TXM-XANES fitting, the nickel absorption K-edge shift was identified as an indicator of the state-of charge, which showed a significant 3 eV shift when charging from open-circuit to 4.2 V (Fig. 7B(b and c)).[91] This concept was used to illustrate the kinetics of charge transport during charging of polycrystalline NMC622 cathode particles complexed with a PEO electrolyte.[91] It was demonstrated that delithiation initially starts at the particle surface and then moves inward driven by a Li^+ vacancy gradient.[91] This inward motion occurs through random pathways due to irregularities in grain packing. Despite anisotropic ion transport in the bulk and the existence of voids at the solid/solid interfaces, the Li^+ concentration became relatively uniform across the particle, as electrochemical forces and diffusion compensated for the initial heterogeneities.[91] However, as the battery undergoes cycling, microcracks form within the cathode particles, resulting in contact loss, localized stress, uneven charge distribution, and rapid capacity fading.[91] This is compared to the charging process in liquid electrolyte LIBs in Fig. 7B(d–f). Here, the conformal solid/liquid interface in these batteries facilitates homogeneous and unrestricted Li^+ transport across the NMC622 particle surface, driven by the high ionic conductivity of the liquid electrolyte. The continuous interface contact ensured uniform charging, forming a Li^+ deficient region on the surface that drove Li^+ vacancies radially inward, resulting in a core–shell delithiation model.

Although determining the state-of-charge alone does not directly indicate degradation, heterogeneous redox reaction fronts caused by phenomena such as contact loss can cause some regions to be inactive while others become overactive. This may lead to degradation, particularly for layered oxide cathodes where locally losing more than 50% of Li^+ introduces an irreversible phase change.[92] *Operando* spectroscopy techniques such as full-field transmission microscopy with X-ray absorption fine structure spectroscopy (XAFS) and hard X-ray photoelectron spectroscopy (HAXPES) are among the most important techniques for realizing state-of-charge imaging.[93,94] These types of studies are often conducted on thin-film cells instead of conventional powder pack SSBs. In thin-film SSBs, the cathode often exhibits well-defined geometry, specific crystallographic orientation, and high initial homogeneity. This makes it easier to design experimental setups aimed at monitoring the temporal evolution of heterogeneities. For instance, in a study by Kiuchi *et al.*,[93] *operando* HAXPES measurements during the charge/discharge of a thin-film SSB cell with the LCO cathode revealed that the Co $2p_{3/2}$ and O 1s peaks exhibited voltage-dependent shifts, broadening, and reversible changes, especially around 3.7–4.2 V (Fig. 8A). These spectral evolutions reflect the phase transition of LCO at different states-of-charge from a p-type semiconductor to a metallic state.[87] In another study, the degradation processes were captured during state-of-charge imaging.[94] This work presented cross-sectional X-ray absorption images and state-of-charge distribution maps of the LCO before and after 100 charge/discharge cycles under accelerated degradation conditions. In order to generate spatially resolved maps of state-of-charge, the incident X-ray was scanned across the absorption edge of Co K-edge. This allowed the authors to realize XAFS imaging during TXM (TXM-XAFS) and use the chemical state of Co as an indicator of state-of-charge. A schematic of the *operando* TXM-XAFS setup used in this study is shown in Fig. 8B(a). As shown in XANES spectra and TXM-XAFS maps recorded from pristine LCO (Fig. 8B(b–d)) during the initial charge/discharge cycle at 1C-rate, the Co valence changed uniformly with the state-of-charge, indicating homogeneous redox activity. Higher oxidation states of Co were associated with a shift of the absorption peak to higher energies in XANES spectra. The cells were then degraded by cycling 100 times at high current density (10C-rate). After degradation, the LCO layer was partially detached from the SSE, especially in areas that experienced repeated state-of-charge transitions. Despite the detachment, Co redox reactions still partially proceeded due to in-plane Li^+ diffusion. However, a high Co valence persisted even in the discharged state, suggesting incomplete relaxation and accumulation of oxidized species during cycling (Fig. 8B(d)).

5. Outlook

Addressing the intricate material interactions at the solid/solid interfaces is essential for optimizing the performance of SSBs, but it necessitates a multiscale approach spanning from the atomic to macroscopic levels.[3] As most interface processes occur with characteristic length scales on the order of nanometers, nanoscale characterization plays a key role in uncovering the fundamental processes driving SSB degradation. Nanoscale techniques such as TEM, SPM, and X-ray tomography have already provided valuable insights into key solid-state processes such as dendrite formation, chemically or mechanically unstable electrolyte/electrode interfaces, and inhomogeneous cathodic reactions. However, significant challenges remain, particularly in imaging sub-surface currents, capturing fast and dynamic processes, extending compatibility to real-world battery testing setups, and gaining a complete view of the complex battery processes by combining multiple non-invasive techniques or measurement modalities.

5.1. Multimodal characterization of battery operation and degradation

Beyond improving spatial and temporal resolution, there is an increasing need for multimodal approaches combining nanoscale imaging of, *e.g.*, current distributions, electrochemical reactivity dynamics, and mechanical properties.[6,7,28] To date, this remains a key obstacle. In this context, integrated setups coupling TEM or XRD with mechanical stress measurements

offer powerful platforms for characterizing the transport kinetics of Li^+ at solid/solid interfaces.[3] Similarly, multimodal methods such as AFM-Raman, AFM-IR, and TXM-XANES are essential for elucidating the mechanistic nature of complex degradational processes within these interfaces.[5] Developing systems that seamlessly integrate nanoscale imaging and multimodal property mapping could greatly improve our understanding of SSB degradation.

5.2. Non-invasive *operando* imaging at the nanoscale

In situ and *operando* imaging setups that directly probe or mimic real-world battery conditions are particularly crucial for optimizing materials and accelerating SSB commercialization. However, the key challenge for most *operando* techniques lies in achieving non-invasive operation as well as the ability to penetrate common battery casings with high spatial and temporal resolution without requiring extensive sample modification.[25] Techniques such as XAS and TXM are increasingly employed for nanoscale characterization of reaction kinetics in electrode materials for SSBs.[25] However, one should note that these methods are currently suffering from drawbacks such as a low signal-to-noise ratio and beam sensitivity.[25] Although SSBs are generally sensitive to beam damage and air exposure, techniques such as high-speed XRD and neutron powder diffraction have proven effective for the non-destructive analysis of buried interfaces.[25] Other tools, such as *in situ* Raman spectroscopy, can also further enhance our understanding of solid-state processes within SSE and electrodes, by distinguishing distinct electrochemical reactions during battery operation.[26]

5.3. Artificial intelligence

Integrating artificial intelligence (AI) and machine learning with 3D morphological characterization techniques, such as FIB–SEM, TEM, and nanoscale tomography, presents an exciting opportunity for detailed characterization of SSB materials and interfaces at the nanoscale. These approaches not only enhance our understanding of complex processes but also uncover previously hidden trends.[6,7,28] AI-driven performance-predictive models, which incorporate various phenomena across multiple length scales, hold great promise for improving SSB design and performance.[27] Such large-scale models can analyze the effects of electrode microstructure on performance, providing valuable insights into material heterogeneities and their impact on cell efficiency.[27] Expanding AI models to include time-dependent phenomena and buried interface dynamics will further enhance their predictive and analyzing capability, enabling the identification of unknown degradation mechanisms and optimizing material design for SSBs.

5.4. Imaging of buried transport of ions and electrons

Currently, there is no consensus on the precise origins of several key degradation phenomena in SSBs, highlighting a critical knowledge gap in how these processes evolve at the nanoscale and how their kinetics can be controlled. Paradoxically, although current flows and electric field evolutions govern the operation and degradation of SSBs, visualizing these sub-surface processes at the nanoscale remains a key challenge. Developing imaging methodologies, like the recently proposed quantum sensing methodology,[32] capable of dynamically tracking the movement of ions and electrons in buried interfaces would represent a significant scientific milestone. Such techniques would enable researchers to monitor the evolution of solid-state degradation processes and identify effective mitigation strategies. The ability to capture such dynamic processes at high spatial and temporal resolution is crucial for understanding the interplay between charge movement, redox reactions, and field distributions that occur within SSBs. Furthermore, these capabilities hold potential for addressing additional key challenges, such as quantifying ionic/electronic conduction across grain boundaries and spatially resolving redox-active elements in complex cathode materials.

5.5. Concluding remarks

SSB development hinges on the integration of advanced nanoscale characterization techniques, multimodal approaches, and cutting-edge computational tools. Emerging multimodal approaches combining nanoscale resolution with functional probing offer a promising solution to uncover the interplay between charge movement, redox reactions, and field distributions, paving the way for safer and more efficient SSBs. By coupling these advancements with a holistic understanding of multiscale battery processes, researchers can accelerate the path toward safer, more efficient, and commercially viable SSB technologies. Despite significant progress, imaging the movement of ions and electrons and capturing fast and dynamic degradation processes remain a challenge, highlighting the need for further advancements in both temporal and spatial resolution, as well as the development of unorthodox multimodal imaging techniques.[3]

Author contributions

MK and DVC conceptualized the review and contributed to the overall structure and design of the manuscript. MK led the writing process and coordinated the manuscript's development. FGT conducted a comprehensive literature review, summarized recent studies, prepared the table in the supplementary section, and created the figures and artwork. All authors collaborated on iterative revisions of the manuscript, co-writing, and ensuring its scientific accuracy. DVC supervised the project and offered critical insights into nanoscale characterization techniques with a focus on battery materials. MK provided expertise in battery materials and battery testing procedures.

Conflicts of interest

There is no conflict of interest to declare

Data availability

No primary research results, software or code have been included and no new data were generated or analyzed as part of this review.

The relevant nanoscale characterization techniques for solid state battery applications, along with their spatial resolution, field of view and complementary methods are provided in the supplementary information (SI). See DOI: **https://doi.org/10.1039/d5nh00009b**.

Acknowledgements

The authors acknowledge the support from the Independent Research Fund Denmark for the Sapere Aude project Solid grant 10.46540/3123-00034B and the Novo Nordisk Foundation NERD Programme: New Exploratory Research and Discovery, Superior Grant NNF21OC0068015. DVC acknowledges the Hans Fischer Fellowship funded by the Technical University of Munich – Institute for Advanced Study, Germany.

References

1 J. Janek and W. G. Zeier, Challenges in speeding up solid-state battery development, *Nat. Energy*, 2023, **8**, 230–240, DOI: **10.1038/s41560-023-01208-9**.

2 J. T. Frith, M. J. Lacey and U. Ulissi, A non-academic perspective on the future of lithium-based batteries, *Nat. Commun.*, 2023, **14**, 420, DOI: **10.1038/s41467-023-35933-2**.

3 S. Sun, C. Z. Zhao, H. Yuan, Y. Lu, J. K. Hu, J. Q. Huang and Q. Zhang, Multiscale understanding of high-energycathodes in solid-state batteries: fromatomic scale to macroscopic scale, *Mater. Futures*, 2022, **1**, 012101, DOI: **10.1088/2752-5724/ac427c**.

4 M. Balaish, J. C. Gonzalez-Rosillo, K. J. Kim, Y. Zhu, Z. D. Hood and J. L. M. Rupp, Processing thin but robust electrolytes for solid-state batteries, *Nat. Energy*, 2021, **6**, 227–239, DOI: **10.1038/s41560-020-00759-5**.

5 M. B. Dixit, J.-S. Park, P. Kenesei, J. Almer and K. B. Hatzell, Status and prospect of in situ and operando characterization of solid-state batteries, *Energy Environ. Sci.*, 2021, **14**, 4672–4711, DOI: **10.1039/D1EE00638J**.

6 M. B. Dixit, W. Zaman, N. Hortance, S. Vujic, B. Harkey, F. Shen, W.-Y. Tsai, V. D. Andrade, X. C. Chen, N. Balke and K. B. Hatzell, Nanoscale Mapping of Extrinsic Interfaces in Hybrid Solid Electrolytes, *Joule*, 2020, **4**(1), 207–221, DOI: **10.1016/j.joule.2019.11.015**.

7 X. Liu, R. Garcia-Mendez, A. R. Lupini, Y. Cheng, Z. D. Hood, F. Han, A. Sharafi, J. C. Idrobo, N. J. Dudney, C. Wang, C. Ma, J. Sakamoto and M. Chi, Local electronic structure variation resulting in Li 'filament' formation within solid electrolytes, *Nat. Mater.*, 2021, **20**, 1485–1490, DOI: **10.1038/s41563-021-01019-x**.

8 E. Truong, S. V. Patel, H. Liu, Y. Chen, V. Lacivita, C. Zhang, I. P. Oyekunle, I. Ojelade, Y. Jin, B. T. Jones, L. J. Miara, V. P. Dravid, H. Gao, R. Kim, Y. Wang and Y.-Y. Hu, Accelerating ion transport in polycrystalline conductors: On pores and grain boundaries, *Sci. Adv.*, 2025, **11**(20), eadt7795, DOI: **10.1126/sciadv.adt7795**.

9 C.-S. Jiang, N. Dunlap, Y. Li, H. Guthrey, P. Liu, S.-H. Lee and M. M. Al-Jassim, Nonuniform Ionic and Electronic Transport of Ceramic and Polymer/Ceramic Hybrid Electrolyte by Nanometer-Scale Operando Imaging for Solid-State Battery, *Adv. Energy Mater.*, 2020, **10**(21), 2000219, DOI: **10.1002/aenm.202000219**.

10 M. S. Diallo, T. Shi, Y. Zhang, X. Peng, I. Shozib, Y. Wang, L. J. Miara, M. C. Scott, Q. H. Tu and G. Ceder, Effect of solid-electrolyte pellet density on failure of solid state batteries, *Nat. Commun.*, 2024, **15**, 858, DOI: **10.1038/s41467-024-45030-7**.

11 L. Frenck, G. K. Sethi, J. A. Maslyn and N. P. Balsara, Factors That Control the Formation of Dendrites and Other Morphologies on Lithium Metal Anodes, *Front. Energy Res.*, 2019, **7**, 115, DOI: **10.3389/fenrg.2019.00115**.

12 K. B. Hatzell, X. C. Chen, C. L. Cobb, N. P. Dasgupta, M. B. Dixit, L. E. Marbella, M. T. McDowell, P. P. Mukherjee, A. Verma, V. Viswanathan, A. S. Westover and W. G. Zeier, Challenges in Lithium Metal Anodes for Solid-State Batteries, *ACS Energy Lett.*, 2020, **5**(3), 922–934, DOI: **10.1021/acsenergylett.9b02668**.

13 A. Jetybayeva, D. S. Aaron, I. Belharouak and M. M. Mench, Critical review on recently developed lithium and non-lithium anode-based solid-state lithium-ion batteries, *J. Power Sources*, 2023, **566**, 232914, DOI: **10.1016/j.jpowsour.2023.232914**.

14 B. Li, Y. Chao, M. Li, Y. Xiao, R. Li, K. Yang, X. Cui, G. Xu, L. Li, C. Yang, Y. Yu, D. P. Wilkinson and J. Zhang, A Review of Solid Electrolyte Interphase (SEI) and Dendrite Formation in Lithium Batteries, *Electrochem. Energy Rev.*, 2023, **6**, 7, DOI: **10.1007/s41918-022-00147-5**.

15 Z. Zhang and W.-Q. Han, From Liquid to Solid-State Lithium Metal Batteries: Fundamental Issues and Recent Developments, *Nano-Micro Lett.*, 2024, **16**, 24, DOI: **10.1007/s40820-023-01234-y**.

16 L. Jia, J. Zhu, X. Zhang, B. Guo, Y. Du and X. Zhuang, Li–Solid Electrolyte Interfaces/Interphases in All-Solid-State Li Batteries, *Electrochem. Energy Rev.*, 2024, **7**, 12, DOI: **10.1007/s41918-024-00212-1**.

17 H. Wu, G. Zheng, N. Liu, T. J. Carney, Y. Yang and Y. Cui, Engineering Empty Space between Si Nanoparticles for Lithium-Ion Battery Anodes, *Nano Lett.*, 2012, **12**, 904–909, DOI: **10.1021/nl203967r**.

18 X. Nie, J. Hu and C. Li, Halide-based solid electrolytes: The history, progress, and challenges, *Interdiscip. Mater.*, 2023, **2**(3), 365–389, DOI: **10.1002/idm2.12090**.

19 X. Han, Y. Gong, K. Fu, X. He, G. T. Hitz, J. Dai, A. Pearse, B. Liu, H. Wang, G. Rubloff, Y. Mo, V. Thangadurai, E. D. Wachsman and L. Hu, Negating interfacial impedance in garnet-based solid-state Li metal batteries, *Nat. Mater.*, 2017, **16**, 572–579, DOI: **10.1038/nmat4821**.

20 R. Guo, G. M. Hobold and B. M. Gallant, The ionic interphases of the lithium anode in solid state batteries, *Curr.*

Opin. Solid State Mater. Sci., 2022, **26**(1), 100973, DOI: 10.1016/j.cossms.2021.100973.

21 P. Minnmann, F. Strauss, A. Bielefeld, R. Ruess, P. Adelhelm, S. Burkhardt, S. L. Dreyer, E. Trevisanello, H. Ehrenberg, T. Brezesinski, F. H. Richter and J. Janek, Designing Cathodes and Cathode Active Materials for Solid-State Batteries, *Adv. Energy Mater.*, 2022, **12**(35), 2201425, DOI: 10.1002/aenm.202201425.

22 J. Cabana, L. Monconduit, D. Larcher and M. R. Palacín, Beyond Intercalation-Based Li-Ion Batteries: The State of the Art and Challenges of Electrode Materials Reacting Through Conversion Reactions, *Adv. Mater.*, 2010, **22**(35), E170–E192, DOI: 10.1002/adma.201000717.

23 C. Chen, M. Jiang, T. Zhou, L. Raijmakers, E. Vezhlev, B. Wu, T. U. Schülli, D. L. Danilov, Y. Wei, R. Eichel and P. H. L. Notten, Interface Aspects in All-Solid-State Li-Based Batteries Reviewed, *Adv. Energy Mater.*, 2021, **11**(13), 2003939, DOI: 10.1002/aenm.202003939.

24 Y. Ren, T. Danner, A. Moy, M. Finsterbusch, T. Hamann, J. Dippell, T. Fuchs, M. Müller, R. Hoft, A. Weber, L. A. Curtiss, P. Zapol, M. Klenk, A. T. Ngo, P. Barai, B. C. Wood, R. Shi, L. F. Wan, T. W. Heo, M. Engels, J. Nanda, F. H. Richter, A. Latz, V. Srinivasan, J. Janek, J. Sakamoto, E. D. Wachsman and D. Fattakhova-Rohlfing, Oxide-Based Solid-State Batteries: A Perspective on Composite Cathode Architecture, *Adv. Energy Mater.*, 2023, **13**(1), 2201939, DOI: 10.1002/aenm.202201939.

25 W. Li, D. M. Lutz, L. Wang, K. J. Takeuchi, A. C. Marschilok and E. S. Takeuchi, Peering into Batteries: Electrochemical Insight Through In Situ and Operando Methodsover Multiple Length Scales, *Joule*, 2021, **5**, 77–88, DOI: 10.1016/j.joule.2020.11.003.

26 D. H. S. Tan, A. Banerjee, Z. Chen and Y. S. Meng, From nanoscale interface characterization to sustainable energy storage usingall-solid-state batteries, *Nat. Nanotechnol.*, 2020, **15**, 170–180, DOI: 10.1038/s41565-020-0657-x.

27 J. Scharf, M. Chouchane, D. P. Finegan, B. Lu, C. Redquest, M. Cheol Kim, W. Yao, A. A. Franco, D. Gostovic, Z. Liu, M. Riccio, F. Zelenka, J. M. Doux and Y. S. Meng, Bridging nano- and microscale X-ray tomography for battery research by leveraging artificial intelligence, *Nat. Nanotechnol.*, 2022, **17**, 446–459, DOI: 10.1038/s41565-022-01081-9.

28 Z. Wang, M. Kotobuki, L. Lu and K. Zeng, Nanoscale characterization of solid electrolyte by Scanning Probe Microscopy techniques, *Electrochim. Acta*, 2020, **334**, 135553, DOI: 10.1016/j.electacta.2019.135553.

29 D. Schäfer, K. Hankins, M. Allion, U. Krewer, F. Karcher, L. Derr, R. Schuster, J. Maibach, S. Mück, D. Kramer, R. Mönig, F. Jeschull, S. Daboss, T. Philipp, G. Neusser, J. Romer, K. Palanisamy, C. Kranz, F. Buchner, R. J. Behm, A. Ahmadian, C. Kübel, I. Mohammad, A. Samoson, R. Witter, B. Smarsly and M. Rohnke, Multiscale Investigation of Sodium-Ion Battery Anodes: Analytical Techniques and Applications, *Adv. Energy Mater.*, 2024, **14**(15), 2302830, DOI: 10.1002/aenm.202302830.

30 M. G. Verde, L. Baggetto, N. Balke, G. M. Veith, J. K. Seo, Z. Wang and Y. S. Meng, Elucidating the Phase Transformation of $Li_4Ti_5O_{12}$ Lithiation at the Nanoscale, *ACS Nano*, 2016, **10**(4), 4312–4321, DOI: 10.1021/acsnano.5b07875.

31 D. V. Christensen, U. Staub, T. R. Devidas, B. Kalisky, K. C. Nowack, J. L. Webb, U. L. Andersen, A. Huck, D. A. Broadway, K. Wagner, P. Maletinsky, T. Van Der Sar, C. R. Du, A. Yacoby, D. Collomb, S. Bending, A. Oral, H. J. Hug, A.-O. Mandru, V. Neu, H. W. Schumacher, S. Sievers, H. Saito, A. A. Khajetoorians, N. Hauptmann, S. Baumann, A. Eichler, C. L. Degen, J. McCord, M. Vogel, M. Fiebig, P. Fischer, A. Hierro-Rodriguez, S. Finizio, S. S. Dhesi, C. Donnelly, F. Büttner, O. Kfir, W. Hu, S. Zayko, S. Eisebitt, B. Pfau, R. Frömter, M. Kläui, F. S. Yasin, B. J. McMorran, S. Seki, X. Yu, A. Lubk, D. Wolf, N. Pryds, D. Makarov and M. Poggio, 2024 roadmap on magnetic microscopy techniques and their applications in materials science, *J. Phys. Mater.*, 2024, **7**, 032501, DOI: 10.1088/2515-7639/ad31b5.

32 S. Pollok, M. Khoshkalam, F. Ghaffari-Tabrizi, F. Kurnia, D. Wang, S. Li, D. B. Bucher, J. L. M. Rupp and D. V. Christensen, Magnetic microscopy for operando imaging of battery dynamics, *Nat. Commun.*, 2025, **16**, 8303, DOI: 10.1038/s41467-025-63409-y.

33 W. Zhang, E. Hosono, D. Asakura, H. Yuzawa, T. Ohigashi, M. Kobayashi, H. Kiuchi and Y. Harada, Chemical-state distributions in charged $LiCoO_2$ cathode particles visualized by soft X-ray spectromicroscopy, *Sci. Rep.*, 2023, **13**, 4639, DOI: 10.1038/s41598-023-30673-1.

34 J. Lim, Y. Li, D. H. Alsem, H. So, S. C. Lee, P. Bai, D. A. Cogswell, X. Liu, N. Jin, Y. Yu, N. J. Salmon, D. A. Shapiro, M. Z. Bazant, T. Tyliszczak and W. C. Chueh, Origin and hysteresis of lithium compositional spatio-dynamics within battery primary particles, *Science*, 2016, **353**, 566–571, DOI: 10.1126/science.aaf4914.

35 H. Zhao, H. D. Deng, A. E. Cohen, J. Lim, Y. Li, D. Fraggedakis, B. Jiang, B. D. Storey, W. C. Chueh, R. D. Braatz and M. Z. Bazant, Learning heterogeneous reaction kinetics from X-ray videos pixel by pixel, *Nature*, 2023, **621**, 289–294, DOI: 10.1038/s41586-023-06393-x.

36 A. J. Merryweather, C. Schnedermann, Q. Jacquet, C. P. Grey and A. Rao, Operando optical tracking of single-particle ion dynamics in batteries, *Nature*, 2021, **594**, 522–528, DOI: 10.1038/s41586-021-03584-2.

37 T. Li, H. Kang, X. Zhou, C. Lim, B. Yan, V. De Andrade, F. De Carlo and L. Zhu, Three-Dimensional Reconstruction and Analysis of All-Solid Li-Ion Battery Electrode Using Synchrotron Transmission X-ray Microscopy Tomography, *ACS Appl. Mater. Interfaces*, 2018, **10**(20), 16927–16931, DOI: 10.1021/acsami.7b18962.

38 K. J. Harry, D. T. Hallinan, D. Y. Parkinson, A. A. MacDowell and N. P. Balsara, Detection of subsurface structures underneath dendrites formed on cycled lithium metal electrodes, *Nat. Mater.*, 2014, **13**, 69–73, DOI: 10.1038/nmat3793.

39 C. Xu, Z. Ahmad, A. Aryanfar, V. Viswanathan and J. R. Greer, Enhanced strength and temperature dependence of mechanical properties of Li at small scales and its implications for Li metal anodes, *Proc. Natl. Acad. Sci. U. S. A.*, 2017, **114**(1), 57–61, DOI: 10.1073/pnas.1615733114.

40 X. Gao, C. A. J. Fisher, T. Kimura, Y. H. Ikuhara, H. Moriwake, A. Kuwabara, H. Oki, T. Tojigamori, R. Huang and Y. Ikuhara, Lithium Atom and A-Site Vacancy Distributions in Lanthanum Lithium Titanate, *Chem. Mater.*, 2013, **25**(9), 1607–1614, DOI: **10.1021/cm3041357**.

41 P. Mukherjee, N. V. Faenza, N. Pereira, J. Ciston, L. F. J. Piper, G. G. Amatucci and F. Cosandey, Surface Structural and Chemical Evolution of Layered $LiNi_{0.8}Co_{0.15}Al_{0.05}O_2$ (NCA) under High Voltage and Elevated Temperature Conditions, *Chem. Mater.*, 2018, **30**(23), 8431–8445, DOI: **10.1021/acs.chemmater.7b05305**.

42 K. He, X. Bi, Y. Yuan, T. Foroozan, B. Song, K. Amine, J. Lu and R. Shahbazian-Yassar, Operando liquid cell electron microscopy of discharge and charge kinetics in lithium-oxygen batteries, *Nano Energy*, 2018, **49**, 338–345, DOI: **10.1016/j.nanoen.2018.04.046**.

43 J. Kasemchainan, S. Zekoll, D. Spencer Jolly, Z. Ning, G. O. Hartley, J. Marrow and P. G. Bruce, Critical stripping current leads to dendrite formation on plating in lithium anode solid electrolyte cells, *Nat. Mater.*, 2019, **18**, 1105–1111, DOI: **10.1038/s41563-019-0438-9**.

44 G. McConohy, X. Xu, T. Cui, E. Barks, S. Wang, E. Kaeli, C. Melamed, X. W. Gu and W. C. Chueh, Mechanical regulation of lithium intrusion probability in garnet solid electrolytes, *Nat. Energy*, 2023, **8**, 241–250, DOI: **10.1038/s41560-022-01186-4**.

45 M. Pasta, D. Armstrong, Z. L. Brown, J. Bu, M. R. Castell, P. Chen, A. Cocks, S. A. Corr, E. J. Cussen, E. Darnbrough, V. Deshpande, C. Doerrer, M. S. Dyer, H. El-Shinawi, N. Fleck, P. Grant, G. L. Gregory, C. Grovenor, L. J. Hardwick, J. T. S. Irvine, H. J. Lee, G. Li, E. Liberti, I. McClelland, C. Monroe, P. D. Nellist, P. R. Shearing, E. Shoko, W. Song, D. S. Jolly, C. I. Thomas, S. J. Turrell, M. Vestli, C. K. Williams, Y. Zhou and P. G. Bruce, 2020 roadmap on solid-state batteries, *J. Phys. Energy*, 2020, **2**, 032008, DOI: **10.1088/2515-7655/ab95f4**.

46 X. Wang, M. Zhang, J. Alvarado, S. Wang, M. Sina, B. Lu, J. Bouwer, W. Xu, J. Xiao, J. G. Zhang, J. Liu and Y. S. Meng, New Insights on the Structure of Electrochemically Deposited Lithium Metal and Its Solid Electrolyte Interphases via Cryogenic TEM, *Nano Lett.*, 2017, **17**(12), 7606–7612, DOI: **10.1021/acs.nanolett.7b03606**.

47 D. H. S. Tan, A. Banerjee, Z. Chen and Y. S. Meng, From nanoscale interface characterization to sustainable energy storage using all-solid-state batteries, *Nat. Nanotechnol.*, 2020, **15**, 170–180, DOI: **10.1038/s41565-020-0657-x**.

48 Z. Zhang, S. Said, K. Smith, R. Jervis, C. A. Howard, P. R. Shearing, D. J. L. Brett and T. S. Miller, Characterizing Batteries by In Situ Electrochemical Atomic Force Microscopy: A Critical Review, *Adv. Energy Mater.*, 2021, **11**(38), 2101518, DOI: **10.1002/aenm.202101518**.

49 C.-S. Jiang, N. Dunlap, Y. Li, H. Guthrey, P. Liu, S.-H. Lee and M. M. Al-Jassim, Nonuniform Ionic and Electronic Transport of Ceramic and Polymer/Ceramic Hybrid Electrolyte by Nanometer-Scale Operando Imaging for Solid-State Battery, *Adv. Energy Mater.*, 2020, **10**(21), 2000219, DOI: **10.1002/aenm.202000219**.

50 Z. Sun, M. Li, B. Xiao, X. Liu, H. Lin, B. Jiang, H. Liu, M. Li, D.-L. Peng and Q. Zhang, In situ transmission electron microscopy for understanding materials and interfaces challenges in all-solid-state lithium batteries, *eTransportation*, 2022, **14**, 100203, DOI: **10.1016/j.etran.2022.100203**.

51 Y. Cheng, L. Zhang, Q. Zhang, J. Li, Y. Tang, C. Delmas, T. Zhu, M. Winter, M.-S. Wang and J. Huang, Understanding all solid-state lithium batteries through in situ transmission electron microscopy, *Mater. Today*, 2021, **42**, 137–161, DOI: **10.1016/j.mattod.2020.09.003**.

52 S. F. Mayer, B. Mercier-Guyon, C. Doublet, A. Fauchier-Magnan, L. R. Mangani, C. Renais, M. Reuter, O. Thompson, L. Trassart and C. Villevieille, Understanding Interphases and Interfaces of BatteryMaterials at the Nanoscale, *Small*, 2025, **21**(34), 2504379, DOI: **10.1002/smll.202504379**.

53 A. Li, D. Shan, C. Lei, S. Xie, K. Pan, J. Li and Y. Liu, Mechanics of electrochemical strain microscopy: Computational simulations and experimental validations, *Int. J. Solids Struct.*, 2021, **219–220**, 188–197, DOI: **10.1016/j.ijsolstr.2021.03.009**.

54 X. Liu, X. Li, H. Li and H. B. Wu, Recent Progress of Hybrid Solid-State Electrolytes for Lithium Batteries, *Chem. – Eur. J.*, 2018, **24**(69), 18293–18306, DOI: **10.1002/chem.201803616**.

55 M. Dirican, C. Yan, P. Zhu and X. Zhang, Composite solid electrolytes for all-solid-state lithium batteries, *Mater. Sci. Eng., R*, 2019, **136**, 27–46, DOI: **10.1016/j.mser.2018.10.004**.

56 P. Colomban, Analysis of Strain and Stress in Ceramic, Polymer and Metal Matrix Composites by Raman Spectroscopy, *Adv. Eng. Mater.*, 2002, **4**(8), 535–542, DOI: **10.1002/1527-2648(20020806)4:8%3C535::AID-ADEM535%3E3.0.CO;2-E**.

57 Z. Ning, D. S. Jolly, G. Li, R. De Meyere, S. D. Pu, Y. Chen, J. Kasemchainan, J. Ihli, C. Gong, B. Liu, D. L. R. Melvin, A. Bonnin, O. Magdysyuk, P. Adamson, G. O. Hartley, C. W. Monroe, T. J. Marrow and P. G. Bruce, Visualizing plating-induced cracking in lithium-anode solid-electrolyte cells, *Nat. Mater.*, 2021, **20**, 1121–1129, DOI: **10.1038/s41563-021-00967-8**.

58 J.-M. Doux, H. Nguyen, D. H. S. Tan, A. Banerjee, X. Wang, E. A. Wu, C. Jo, H. Yang and Y. S. Meng, Stack Pressure Considerations for Room-Temperature All-Solid-State Lithium Metal Batteries, *Adv. Energy Mater.*, 2020, **10**(1), 1903253, DOI: **10.1002/aenm.201903253**.

59 J. A. Lewis, F. J. Q. Cortes, Y. Liu, J. C. Miers, A. Verma, B. S. Vishnugopi, J. Tippens, D. Prakash, T. S. Marchese, S. Y. Han, C. Lee, P. P. Shetty, H.-W. Lee, P. Shevchenko, F. De Carlo, C. Saldana, P. P. Mukherjee and M. T. McDowell, Linking void and interphase evolution to electrochemistry in solid-state batteries using operando X-ray tomography, *Nat. Mater.*, 2021, **20**, 503–510, DOI: **10.1038/s41563-020-00903-2**.

60 Y. He, X. Ren, Y. Xu, M. H. Engelhard, X. Li, J. Xiao, J. Liu, J.-G. Zhang, W. Xu and C. Wang, Origin of lithium whisker formation and growth under stress, *Nat. Nanotechnol.*, 2019, **14**, 1042–1047, DOI: **10.1038/s41565-019-0558-z**.

61 S. Kim, C. Jung, H. Kim, K. E. Thomas-Alyea, G. Yoon, B. Kim, M. E. Badding, Z. Song, J. Chang, J. Kim, D. Im

and K. Kang, The Role of Interlayer Chemistry in Li-Metal Growth through a Garnet-Type Solid Electrolyte, *Adv. Energy Mater.*, 2020, **10**, 1903993, DOI: 10.1002/aenm.201903993.

62 S. H. Kim, K. Kim, H. Choi, D. Im, S. Heo and H. S. Choi, In situ observation of lithium metal plating in a sulfur-based solid electrolyte for all-solid-state batteries, *J. Mater. Chem. A*, 2019, **7**, 13650–13657, DOI: 10.1039/C9TA02614B.

63 N. Seitzman, H. Guthrey, D. B. Sulas, H. A. S. Platt, M. Al-Jassim and S. Pylypenko, Toward All-Solid-State Lithium Batteries: Three-Dimensional Visualization of Lithium Migration in β-Li_3PS_4 Ceramic Electrolyte, *J. Electrochem. Soc.*, 2018, **165**, A3732–A3737, DOI: 10.1149/2.0301816jes.

64 P. Pietsch and V. Wood, X-Ray Tomography for Lithium Ion Battery Research: A Practical Guide, *Annu. Rev. Mater. Res.*, 2017, **47**, 451–479, DOI: 10.1146/annurev-matsci-070616-123957.

65 Z. Liang, Y. Xiang, K. Wang, J. Zhu, Y. Jin, H. Wang, B. Zheng, Z. Chen, M. Tao, X. Liu, Y. Wu, R. Fu, C. Wang, M. Winter and Y. Yang, Understanding the failure process of sulfide-based all-solid-state lithium batteries via operando nuclear magnetic resonance spectroscopy, *Nat. Commun.*, 2023, **14**, 259, DOI: 10.1038/s41467-023-35920-7.

66 J. Morey, J.-B. Ledeuil, H. Martinez and L. Madec, Operando Auger/XPS using an electron beam to reveal the dynamics/morphology of Li plating and interphase formation in solid-state batteries, *J. Mater. Chem. A*, 2023, **11**, 9512–9520, DOI: 10.1039/D3TA00386H.

67 B. Aktekin, E. Kataev, L. M. Riegger, R. Garcia-Diez, Z. Chalkley, J. Becker, R. G. Wilks, A. Henss, M. Bär and J. Janek, Operando Photoelectron Spectroscopy Analysis of Li_6PS_5Cl Electrochemical Decomposition Reactions in Solid-State Batteries, *ACS Energy Lett.*, 2024, **9**(7), 3492–3500, DOI: 10.1021/acsenergylett.4c01072.

68 E. Flores, P. Novák and E. J. Berg, *In situ* and *Operando* Raman Spectroscopy of Layered Transition Metal Oxides for Li-ion Battery Cathodes, *Front. Energy Res.*, 2018, **6**, 82, DOI: 10.3389/fenrg.2018.00082.

69 D. Yun, S. Kim, S. Heo, H. Choi, J. Baik, J. Chung, S. Park, D. Yu, J. Lee, S. Kang, C. Jung and D. Ko, Understanding the Role of Metal Interlayers in All-Solid-Electrolyte Batteries Using Operando X-Ray Photoelectron Spectroscopy, *Adv. Energy Mater.*, 2024, **14**(34), 2401473, DOI: 10.1002/aenm.202401473.

70 K. Aruchamy, S. Ramasundaram, S. Divya, M. Chandran, K. Yun and T. H. Oh, Gel Polymer Electrolytes: Advancing Solid-State Batteries for High-Performance Applications, *Gels*, 2023, **9**(7), 585, DOI: 10.3390/gels9070585.

71 R. Li, R. Deng, Z. Wang, Y. Wang, G. Huang, J. Wang and F. Pan, The challenges and perspectives of developing solid-state electrolytes for rechargeable multivalent battery, *J. Solid State Electrochem.*, 2023, **27**, 1291–1327, DOI: 10.1007/s10008-023-05426-9.

72 O. Sheng, J. Zheng, Z. Ju, C. Jin, Y. Wang, M. Chen, J. Nai, T. Liu, W. Zhang, Y. Liu and X. Tao, In Situ Construction of a LiF-Enriched Interface for Stable All-Solid-State Batteries and its Origin Revealed by Cryo-TEM, *Adv. Mater.*, 2020, **32**(34), 2000223, DOI: 10.1002/adma.202000223.

73 M. Kühne, F. Börrnert, S. Fecher, M. Ghorbani-Asl, J. Biskupek, D. Samuelis, A. V. Krasheninnikov, U. Kaiser and J. H. Smet, Reversible superdense ordering of lithium between two graphene sheets, *Nature*, 2018, **564**, 234–239, DOI: 10.1038/s41586-018-0754-2.

74 J. Asenbauer, T. Eisenmann, M. Kuenzel, A. Kazzazi, Z. Chen and D. Bresser, The success story of graphite as a lithium-ion anode material – fundamentals, remaining challenges, and recent developments including silicon (oxide) composites, *Sustainable Energy Fuels*, 2020, **4**, 5387–5416, DOI: 10.1039/D0SE00175A.

75 M. Bendayan and E. Paransky, Low Voltage Transmission Electron Microscopy in Cell Biology, *Prog. Histochem. Cytochem.*, 2015, **50**(1–2), 1–10, DOI: 10.1016/j.proghi.2015.05.001.

76 K. Yang, L. Jia, X. Liu, Z. Wang, Y. Wang, Y. Li, H. Chen, B. Wu, L. Yang and F. Pan, Revealing the anion intercalation behavior and surface evolution of graphite in dual-ion batteries via in situ AFM, *Nano Res.*, 2020, **13**, 412–418, DOI: 10.1007/s12274-020-2623-1.

77 S. Müller, P. Pietsch, B.-E. Brandt, P. Baade, V. De Andrade, F. De Carlo and V. Wood, Quantification and modeling of mechanical degradation in lithium-ion batteries based on nanoscale imaging, *Nat. Commun.*, 2018, **9**, 2340, DOI: 10.1038/s41467-018-04477-1.

78 X. H. Liu, H. Zheng, L. Zhong, S. Huang, K. Karki, L. Q. Zhang, Y. Liu, A. Kushima, W. T. Liang, J. W. Wang, J.-H. Cho, E. Epstein, S. A. Dayeh, S. T. Picraux, T. Zhu, J. Li, J. P. Sullivan, J. Cumings, C. Wang, S. X. Mao, Z. Z. Ye, S. Zhang and J. Y. Huang, Anisotropic Swelling and Fracture of Silicon Nanowires during Lithiation, *Nano Lett.*, 2011, **11**(8), 3312–3318, DOI: 10.1021/nl201684d.

79 X. Zhao and G. Ceder, Zero-strain cathode materials for Li-ion batteries, *Joule*, 2022, **6**(12), 2683–2685, DOI: 10.1016/j.joule.2022.11.012.

80 G. Vardar, W. J. Bowman, Q. Lu, J. Wang, R. J. Chater, A. Aguadero, R. Seibert, J. Terry, A. Hunt, I. Waluyo, D. D. Fong, A. Jarry, E. J. Crumlin, S. L. Hellstrom, Y.-M. Chiang and B. Yildiz, Structure, Chemistry, and Charge Transfer Resistance of the Interface between $Li_7La_3Zr_2O_{12}$ Electrolyte and $LiCoO_2$ Cathode, *Chem. Mater.*, 2018, **30**(18), 6259–6276, DOI: 10.1021/acs.chemmater.8b01713.

81 Y. Gong, J. Zhang, L. Jiang, J.-A. Shi, Q. Zhang, Z. Yang, D. Zou, J. Wang, X. Yu, R. Xiao, Y.-S. Hu, L. Gu, H. Li and L. Chen, In Situ Atomic-Scale Observation of Electrochemical Delithiation Induced Structure Evolution of $LiCoO_2$ Cathode in a Working All-Solid-State Battery, *J. Am. Chem. Soc.*, 2017, **139**(12), 4274–4277, DOI: 10.1021/jacs.6b13344.

82 C. Wang, S. Hwang, M. Jiang, J. Liang, Y. Sun, K. Adair, M. Zheng, S. Mukherjee, X. Li, R. Li, H. Huang, S. Zhao, L. Zhang, S. Lu, J. Wang, C. V. Singh, D. Su and X. Sun, Deciphering Interfacial Chemical and Electrochemical Reactions of Sulfide-Based All-Solid-State Batteries, *Adv. Energy Mater.*, 2021, **11**(24), 2100210, DOI: 10.1002/aenm.202100210.

83 Z. Wang, D. Santhanagopalan, W. Zhang, F. Wang, H. L. Xin, K. He, J. Li, N. Dudney and Y. S. Meng, In Situ

STEM-EELS Observation of Nanoscale Interfacial Phenomena in All-Solid-State Batteries, *Nano Lett.*, 2016, **16**(6), 3760–3767, DOI: **10.1021/acs.nanolett.6b01119**.

84 Z. Zhao, Z. Wen, X. Liu, H. Yang, S. Chen, C. Li, H. Lv, F. Wu, B. Wu and D. Mu, Tuning a compatible interface with LLZTO integrated on cathode material for improving NCM811/LLZTO solid-state battery, *Chem. Eng. J.*, 2021, **405**, 127031, DOI: **10.1016/j.cej.2020.127031**.

85 X. Liu, Y. Cheng, Y. Su, F. Ren, J. Zhao, Z. Liang, B. Zheng, J. Shi, K. Zhou, Y. Xiang, J. Zheng, M.-S. Wang, J. Huang, M. Shao and Y. Yang, Revealing the surface-to-bulk degradation mechanism of nickel-rich cathode in sulfide all-solid-state batteries, *Energy Storage Mater.*, 2023, **54**, 713–723, DOI: **10.1016/j.ensm.2022.11.019**.

86 S. Jeon, G. Lim, H. Lee, H. Park, M. K. Cho, C. Kim, Y. Lee, J. Kim, M. Kwon, J. Yoo, H. Jeong, J. Kim, S. Yu, M. Lee, J. Kim and J. Hong, Reduction-Induced Oxygen Loss: the Hidden Surface Reconstruction Mechanism of Layered Oxide Cathodes in Lithium-Ion Batteries, *Adv. Energy Mater.*, 2025, **15**(12), 2404193, DOI: **10.1002/aenm.202404193**.

87 B. Lelotte, C. A. F. Vaz, L. Xu, C. N. Borca, T. Huthwelker, V. Pelé, C. Jordy, L. Gubler and M. El Kazzi, Spatio-Chemical Deconvolution of the $LiNi_{0.6}Co_{0.2}Mn_{0.2}O_2$/$Li_6PS_5Cl$ Interphase Layer in All-Solid-State Batteries Using Combined X-ray Spectroscopic Methods, *ACS Appl. Mater. Interfaces*, 2025, **17**(9), 14645–14659, DOI: **10.1021/acsami.4c19857**.

88 W. Zhong, J. Tao, Y. Chen, R. G. White, L. Zhang, J. Li, Z. Huang and Y. Lin, Unraveling the evolution of Cathode–Solid electrolyte interface using operando X-ray Photoelectron spectroscopy, *Adv. Powder Mater.*, 2024, **3**(3), 100184, DOI: **10.1016/j.apmate.2024.100184**.

89 P. Minnmann, F. Strauss, A. Bielefeld, R. Ruess, P. Adelhelm, S. Burkhardt, S. L. Dreyer, E. Trevisanello, H. Ehrenberg, T. Brezesinski, F. H. Richter and J. Janek, Designing Cathodes and Cathode Active Materials for Solid-State Batteries, *Adv. Energy Mater.*, 2022, **12**(35), 2201425, DOI: **10.1002/aenm.202201425**.

90 T. Shi, Y.-Q. Zhang, Q. Tu, Y. Wang, M. C. Scott and G. Ceder, Characterization of mechanical degradation in an all-solid-state battery cathode, *J. Mater. Chem. A*, 2020, **8**, 17399–17404, DOI: **10.1039/D0TA06985J**.

91 S. Lou, Q. Liu, F. Zhang, Q. Liu, Z. Yu, T. Mu, Y. Zhao, J. Borovilas, Y. Chen, M. Ge, X. Xiao, W.-K. Lee, G. Yin, Y. Yang, X. Sun and J. Wang, Insights into interfacial effect and local lithium-ion transport in polycrystalline cathodes of solid-state batteries, *Nat. Commun.*, 2020, **11**, 5700, DOI: **10.1038/s41467-020-19528-9**.

92 M. Mikami, J. Saito, T. Ochiai, M. Takahashi, T. Takahashi, Y. Momma, K. Kuriki, R. Wada, K. Yokomizo, G. Kobayashi, S. Komaba and S. Yamazaki, Controlling lithium cobalt oxide phase transition using molten fluoride salt for improved lithium-ion batteries, *Commun. Mater.*, 2024, **5**, 108, DOI: **10.1038/s43246-024-00543-y**.

93 H. Kiuchi, K. Hikima, K. Shimizu, R. Kanno, F. Toshiharu and E. Matsubara, Operando hard X-ray photoelectron spectroscopy of $LiCoO_2$ thin film in an all-solid-state lithium ion battery, *Electrochem. Commun.*, 2020, **118**, 106790, DOI: **10.1016/j.elecom.2020.106790**.

94 N. Ishiguro, T. Totsuka, H. Uematsu, O. Sekizawa, K. Yamamoto, Y. Iriyama and Y. Takahashi, Comprehensive Operando Visualization of the Electrochemical Events in the Cathode/Anode Layers in Thin-Film-Type All-Solid-State Lithium-Ion Batteries, *ACS Appl. Energy Mater.*, 2023, **6**(15), 8306–8315, DOI: **10.1021/acsaem.3c01441**.